

~~CONFIDENTIAL~~

~~UNCLASSIFIED~~

~~NACA~~

RESEARCH MEMORANDUM

LANGLEY 9-INCH SUPERSONIC TUNNEL TESTS OF SEVERAL
MODIFICATIONS OF A SUPERSONIC MISSILE HAVING
TANDEM CRUCIFORM LIFTING SURFACES
THREE-COMPONENT DATA RESULTS OF MODELS HAVING
RATIOS OF WING SPAN TO TAIL SPAN EQUAL TO 1

By Robert W. Rainey

Langley Aeronautical Laboratory
Langley Field, Va.

CLASSIFIED DOCUMENT

This document contains classified information affecting the National Defense of the United States within the meaning of the Espionage Act, USC 50-31 and 32. Its transmission or the revelation of its contents in any manner to an unauthorized person is prohibited by law.
Information so classified may be imparted only to persons in the military and naval services of the United States, appropriate civilian officers and employees of the Federal Government who have a legitimate interest therein, and to United States citizens of known loyalty and discretion who of necessity must be informed thereof.

NATIONAL ADVISORY COMMITTEE FOR AERONAUTICS

WASHINGTON
~~UNCLASSIFIED~~

~~CONFIDENTIAL~~

NACA LIBRARY
LANGLEY AERONAUTICAL LABORATORY
Langley Field, Va.

NACA RM L9L30

CLASSIFICATION CHANGED

UNCLASSIFIED

To

By authority of *NRA #17*
Signature
Date 3/18/60
95A



NATIONAL ADVISORY COMMITTEE FOR AERONAUTICS

RESEARCH MEMORANDUM

LANGLEY 9-INCH SUPERSONIC TUNNEL TESTS OF SEVERAL
MODIFICATIONS OF A SUPERSONIC MISSILE HAVING
TANDEM CRUCIFORM LIFTING SURFACESTHREE-COMPONENT DATA RESULTS OF MODELS HAVING
RATIOS OF WING SPAN TO TAIL SPAN EQUAL TO 1

By Robert W. Rainey

SUMMARY

Tests were made in the Langley 9-inch supersonic tunnel to investigate the factors that determine the magnitude of the wing-tail interference effects on the static longitudinal stability of supersonic missile configurations having low-aspect-ratio, tandem, cruciform lifting surfaces and to develop a missile configuration with a minimum variation in static margin due to wing-tail interference effects.

This paper presents lift, drag, and pitching-moment data for several configurations of a missile having equal wing and tail spans. These configurations included variations in interdigitation angle, wing plan form, and body length. Also, data from some tests of elements and various combinations of elements of the missile configurations, made to permit an evaluation of the interference effects, are presented. These data were obtained over an angle-of-attack range of -5° to 15° and over a Mach number range from 1.62 to 2.40. Most of the data, however, were obtained at a Mach number of 1.93. The Reynolds number at $M = 1.93$ was 0.27×10^6 based on the maximum body diameter. The data show the effects of wing-tail interference on the static longitudinal stability of these missile configurations.

INTRODUCTION

In developing a missile with tandem, low-aspect-ratio, cruciform lifting surfaces, one of the problems encountered is the effects of



wing-tail interference upon the static longitudinal stability of the missile. The predominant effect is associated with the changes in the induced flow field at the tail as the angle of attack is varied causing nonlinear changes in the resultant downwash over the tail surface. This nonlinearity results in a change in the static margin and, in the case of a guided missile, would add complications to the control systems.

The solution of this wing-tail-interference problem requires a knowledge of the aerodynamic characteristics of the individual components and their effects upon each other when the components are combined. The theoretical treatment of the general problem of wing-tail interference is exceedingly difficult. In order to make available data for general information and guidance in missile design, an experimental investigation was made in the Langley 9-inch supersonic tunnel to determine the wing-tail interference effects on the pitching moments of various body-wing-tail combinations with the specific purpose of developing a missile configuration with a minimum variation of static margin with angle of attack and angle of roll. At the start of this investigation a "basic" missile configuration with a wing-tail-span ratio equal to 1 and with low-aspect-ratio, cruciform, tandem lifting surfaces was established. For this configuration three-component force data were obtained. The results of these tests and of tests of the basic model with changes in interdigitation angle and tail length established the factors which determine the magnitude of the wing-tail interference effects upon the pitching moment. Further modifications were then made in order to reduce the effects of wing-tail interference.

In the present paper are presented the lift, drag, and pitching-moment characteristics of the first series of tests of the basic configuration ($B_1W_1^{45}T_1$) and of the basic configuration with variations in interdigitation angle, wing plan form, and body length. These modifications were selected initially to vary the location of the induced flow field behind the wing with respect to the tail surfaces (by making variations in interdigitation angle and body length) and to vary the strengths of the local regions of vorticity behind the wing in which the tail surfaces operated by varying the wing plan form (which in turn varied the wing spanwise loading, of which the resultant downwash behind the wing is a function). Also included in the present paper are results of breakdown or component tests of the various elements and combinations of elements of the basic and modified versions of the basic missile. With these results it is possible to obtain the characteristics of one component in the presence of another or others. These tests were made in the Mach number range of 1.62 to 2.40 at Reynolds numbers from 0.362×10^6 to 0.262×10^6 per inch, respectively. In order to expedite publication of these data, no analyses of results are presented.

In two subsequent papers are to be presented the results of tests of configurations upon which further modifications were made, namely, variations in wing-tail-span ratio, tail leading-edge sweep angle, and wing and tail plan forms.

SYMBOLS

S	maximum body cross-sectional area
d	maximum body diameter
C_L	lift coefficient $\left(\frac{L}{qS}\right)$
C_m	pitching-moment coefficient, moments taken about center of gravity, see figure 1 $\left(\frac{M}{qSd}\right)$
C_D	drag coefficient $\left(\frac{D}{qS}\right)$
q	dynamic pressure $\left(\frac{\rho V^2}{2}\right)$
α	angle of attack, degrees
i_t	tail incidence angle, degrees
δ	control-surface deflection, degrees
ϕ	angle of roll of model relative to angle-of-attack plane, positive when model, viewed from rear, is rotated clockwise ($\phi = 0^\circ$ when opposite tail panels are in angle-of-attack plane)
θ	angle between a plane through opposite tail panels and a plane through opposite wing panels, positive when wings are rotated clockwise with respect to tails, when the model is viewed from rear. The angle θ is always less than 90° , and its value appears as the superscript for W in the model configuration designations. When θ values (superscripts on W) are indicated for BW configurations, the subtracted tail is assumed to be present at $\phi = 0^\circ$.
B	configuration of body

BT configuration of body and tails
 BW configuration of body and wings
 BWT configuration of body, wings, and tails

Subscripts:

1, 2, 3 refers to a particular body, wing, or tail plan form (see fig. 1)
 T body has internal taper at stern (see fig. 2)
 C conduit covers are in place on body
 e control surfaces on opposite tail panels deflected in same direction as elevators
 a control surfaces on opposite tail panels deflected in opposite direction as ailerons

Superscripts:

Numerical superscript for W gives value of θ . (See definition of θ .)

APPARATUS AND TEST PROCEDURE

Wind Tunnel

All tests were conducted in the Langley 9-inch supersonic tunnel which is a continuous-operation closed-circuit type in which the stream pressure, temperature, and humidity conditions can be controlled and regulated. Different test Mach numbers are provided by interchanging nozzle blocks which form test sections approximately 9 inches square. Throughout the present tests, the moisture content in the tunnel was kept sufficiently low so that the effects of condensation in the supersonic nozzle were negligible. Eleven fine-mesh turbulence-damping screens are provided in the relatively large area settling chamber just ahead of the supersonic nozzle. A schlieren optical system is provided for qualitative visual flow observations.

Test Setup and Models

A schematic drawing of the model installation in the tunnel is shown in figure 3. The model center-of-gravity or moment reference.

~~CONFIDENTIAL~~

location was kept fixed on the axis of the tunnel as the angle of attack was varied. Mechanically, the reference was kept fixed by translating the shield assembly in the angle-of-attack plane with respect to the tunnel and translating the cross bar and angle-of-attack sector with respect to the floating frame of the balance system. Before each set of readings at a given angle of attack, the gap between the base of the model and the movable windshield was carefully adjusted to a constant opening around the periphery. The pressure inside the box enclosing the balance and the sting was held at a constant value (just below stream pressure) throughout the tests at each Mach number, except when effects of variable box pressure were investigated. It is seen in figure 3 from the estimated limits of the critical disturbance due to the model and its reflections that, with the system employed in which the effective center of rotation of the model can be selected, the axis of the body tends to stay symmetrically boxed in by these disturbances without interference. In this way, the longest possible model for a given tunnel size and Mach number can be utilized.

Dimensions, details, and designations of the various models used in the tests are given in figures 1 and 2. The basic model upon which modifications were made was designated $B_1W_1^{45}T_1$. The actual models were found generally to be accurate within about ± 0.002 inch of the dimensions shown. As seen in the cross-sectional view of the model in figure 2, the various wings and tails of each complete configuration could be changed or located differently with respect to each other on the body or could be omitted. Also, the body lengths could be changed by inserting sections in the cylindrical portion. All of the elements and combinations of elements of the models tested may be seen in the index of figures. The pair of conduit covers designated by the subscript C were mounted on the side of the body in a plane $22\frac{10}{2}$ from the angle-of-attack plane for $\phi = 0^\circ$. These covers were rectangular in section (0.04 in. by 0.12 in. by 3.50 in.) and mounted with their leading edges 4.87 inches from the body nose.

For all tests of the model with wings or tails, the cruciform arrangement shown in figure 1 was used with the exception that, for test 42, runs 71, 72; 74, 75, 82, 83, and 84, a single pair of tail panels always normal to the angle-of-attack plane was employed. These runs were made to obtain integrated downwash values at the tail by the build-up procedure and each of three different sets of tails was set at different incidence angles. These tails had no movable elevators.

The internal taper at the stern of the body shown in figure 2 was found necessary to remove the largest part of an extraneous moment at zero angle of attack which appeared as the tests progressed. This taper is discussed in the section entitled "Presentation of Data." It may be seen that the stern of the body was tapered for all runs after test 44, run 63.

PRECISION OF DATA

For all of the test Mach numbers, pressure surveys throughout the test section have shown the stream to be uniform within a maximum variation in Mach number of ± 0.01 . Less detailed angle surveys have indicated negligible flow deviations and, also, from past experience, both zero moment and zero lift are generally realized for symmetrical configurations at zero angle of attack. These points are brought out to emphasize the fact that for the present tests when an unexpected moment or lift appears at zero angle of attack, several possibilities exist; namely, the configuration is asymmetrical, the flow about the symmetrical configuration is asymmetrical, and/or an extraneous force appears as a result of the flow around the support system or windshield. For the present tests, the most likely reason for an extraneous moment or lift at zero angle of attack is a misaligned (other than zero angle with respect to the body axis) wing or tail panel. Measurements of the various wings and tails indicated that inadvertent incidences are present which contributed to the various lifts and moments evident at zero angle of attack.

All of the three force components were measured by means of self-balancing mechanical scales. A conservative estimate of the maximum probable errors in these measurements is given in the following table:

Mach number \ Coefficient	1.62	1.93	2.40
C_L	± 0.001	± 0.001	± 0.001
C_D	$\pm .003$	$\pm .003$	$\pm .004$
C_m	$\pm .013$	$\pm .014$	$\pm .020$

Reference to the data will show that these errors are probably very small as compared with the scatter about a mean curve or displacement of a mean curve arising from other possible errors.

Angles of attack with respect to each other in a given run are accurate to $\pm 0.01^\circ$. The errors in initially referencing the body axis parallel to the air stream are somewhat higher and may be up to 0.03° .

Angle settings of the elevators are in doubt to between 0.1° and 0.2° . This relatively large error arises from the difficulties associated with the small size of each movable surface. Also, the method

of securing each surface at a given angle was such that the elevator might slip during a run an angle of the order of 0.1° .

Tail-incidence-angle measurements, while not assessed exactly, are believed accurate within less than $\pm 0.05^\circ$.

PRESENTATION OF DATA

The data are presented in figures 4 to 26. An index precedes the figures in which the figures are listed in order of presentation. The figures are grouped according to Mach number, and for each Mach number, the data are approximately in order of the model buildup, that is, first body alone, then body and wing, and so forth. Included in each data figure are the test and run numbers; these are presented because certain geometric variables are common to consecutive tests and also for ease in referring to the individual tests; for instance, the tapered stern in the body applies to all tests after test 44, run 63.

It should be emphasized, in regard to the lift and moment at zero angle of attack for symmetrical configurations, that the elevator settings, although intended to be constant and at a value near 0° (for those tests other than elevator-effectiveness tests), were variable because the mechanical means for locking the elevators was not absolutely positive. Thus the elevator settings changed slightly from a constant value near 0° every time the model was disassembled and reassembled into another configuration. The elevators were finally fixed by soldering them in place so that for test 44, run 190 and thereafter, changes in elevator deflections were not involved between or during runs. Also, in observing the moment or lift at zero angle of attack, the rather large values encountered in the body-tail and body-wing-tail configurations were caused by inadvertent tail incidences.

An interesting result of the tests that appears significant is the effects of small protuberances on the measured characteristics. One aspect of this effect is illustrated in figure 25. The mirror referred to in figure 25 was used for optical angle-of-attack indication and was mounted near the center-of-gravity location. It was noted that the small protrusion of the mirror (about 0.004 in.) led to asymmetries in the drag and moment curves for the body alone and to a displacement of the lift and moment curves at zero angle of attack. The results of figure 25 show that both the asymmetries and displacements at zero angle of attack are reduced by making the mirror flush or by moving the point of disturbance near the rear of the body. Other tests (not shown), in which small protrusions were placed on alternate sides of the body and at different forward and rearward locations along the body, showed that the asymmetry in the drag curves reversed when the protrusion was moved from one side

to the other and that the magnitude of the asymmetry decreased as the protrusion was moved back on the body. It was also observed that for configurations with wings or tails, a small nick in the leading edge of one of the surfaces introduced the same effects as a protrusion on the body. All of these observations suggested that the boundary-layer flow over the body was laminar and transition was readily induced. It appears probable that the wings lead to transition of the laminar flow over the body behind the wings but do not lead to transition of the flow over the tails since nicks in the tails were also observed to give asymmetries.

The effects of varying both the gap and the box pressure relative to stream pressure were investigated. It was found that with the gap setting used throughout the tests, variations in box pressure from several percent below to several percent above stream pressure did not affect the model characteristics. In regard to the drag, this means that the fore drag of each configuration was independent of box pressure and that the base pressure was equal to the box pressure. All drag results were corrected to free-stream base pressure.

As the tests progressed, it was noted at approximately the time of the start of test 44 that a displacement of the moment at zero angle of attack which was larger than that previously experienced was present. Exhaustive tests to determine the source of this displacement were made. It was finally found that tapering the stern of the body internally removed the largest part of the displacement. This result suggested that the extraneous force arose as a result of an asymmetrical flow inside the body that led to a transverse pressure force internally at the stern.

Lastly, the moment reversals near zero angle of attack for the in-line (BW^0T) configurations and between 6° and 8° for the interdigitated ($\theta \neq 0^\circ$) configurations ($BW^{45}T$) appear characteristic for low-aspect-ratio configurations in which the ratio of tail or wing span to body diameter is small and the tail span approximately equals the wing span. It appears that these characteristics can be roughly explained

by first-order considerations of the downwash field as the vortex sheet moves and distorts with respect to the tails.

Langley Aeronautical Laboratory
National Advisory Committee for Aeronautics
Langley Field, Va.

INDEX OF FIGURES

Figure	Mach number	Figure legends
1	----	Model dimensions and center-of-gravity location
2	----	Cross section of model body and stern detail
3	----	Model installation in tunnel showing approximate disturbance limits
4	1.93	$W_1^{4.5}$ increments on B_1 T_1 increments on B_1 Effect of tapered stern on B_1 and $B_1 T_1$ $B_1 W_1^{4.5} T_1$
5	1.93	Basic B_{2c} characteristics $W_1^{4.5}$ increments on B_{2c} T_1 increments on B_{2c}
6	1.93	W_1^0 increments on B_{2c} $B_{2c} W_1^{4.5} T_1$
7	1.93	Effect of elevator deflection on $B_{2c} W_1^{4.5} T_1$
8	1.93	Basic B_2 characteristics $W_1^{4.5}$ increments on B_2
9	1.93	$B_2 W_1^{6.0} T_1$ $B_2 W_1^{7.0} T_1$ at roll angles
10	1.93	Effect of varying tail incidence angle in presence of B_2 (to obtain integrated downwash at tail)
11	1.93	Effect of varying tail incidence angle in presence of $B_2 W_1^{4.5}$ (to obtain integrated downwash at tail)
12	1.93	Basic B_{2T} characteristics
13	1.93	$W_1^{4.5}$ increments on B_{2T} at roll angles
14	1.93	$W_2^{4.5}$ increments on B_{2T} W_2^0 increments on B_{2T} $W_3^{4.5}$ increments on B_{2T}
15	1.93	$B_{2T} W_1^{4.5} T_1$ at roll angles
16	1.93	$B_{2T} W_1^{3.0} T_1$ at roll angles
17	1.93	$B_{2T} W_2^{4.5} T_1$ at roll angles
18	1.93	$B_{2T} W_2^0 T_1$ at roll angles
19	1.93	$B_{2T} W_3^{4.5} T_1$ at roll angles
20	1.93	$B_{2T} W_3^0 T_1$ at roll angles
21	1.62	Basic B_{2c} characteristics $W_1^{4.5}$ increments on B_{2c}
22	1.62	Basic B_2 characteristics W_1 increments on B_2 $B_1 W_1^{4.5} T_1$
23	1.62	Effect of elevator deflection on $B_2 T_1$
24	1.62	$B_2 W_1^{4.5} T_1$ $B_{2c} W_1^{2.0} T_1$ $B_{2c} W_1^{3.5} T_1$ $B_{2c} W_1^{4.5} T_1$ $B_{2c} W_1^{4.5} T_1$ ($\alpha_a = 4.4^\circ$)
25	2.40	B_2 with variations in angle-of-attack mirror
26	2.40	$W_1^{4.5}$ increments on B_2 T_1 increments on B_2 $B_2 W_1^{4.5} T_1$

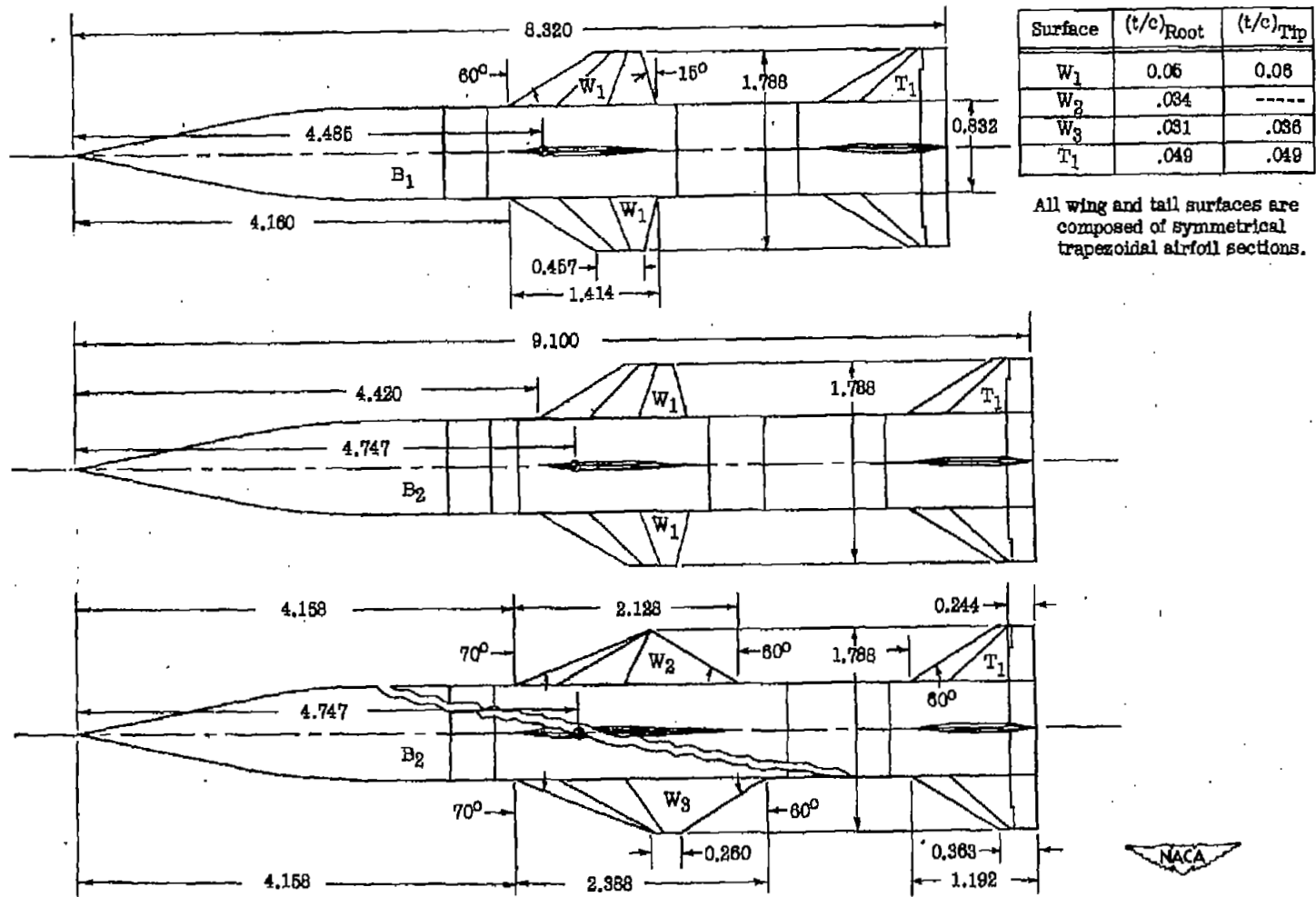


Figure 1.- Model dimensions and center-of-gravity location.

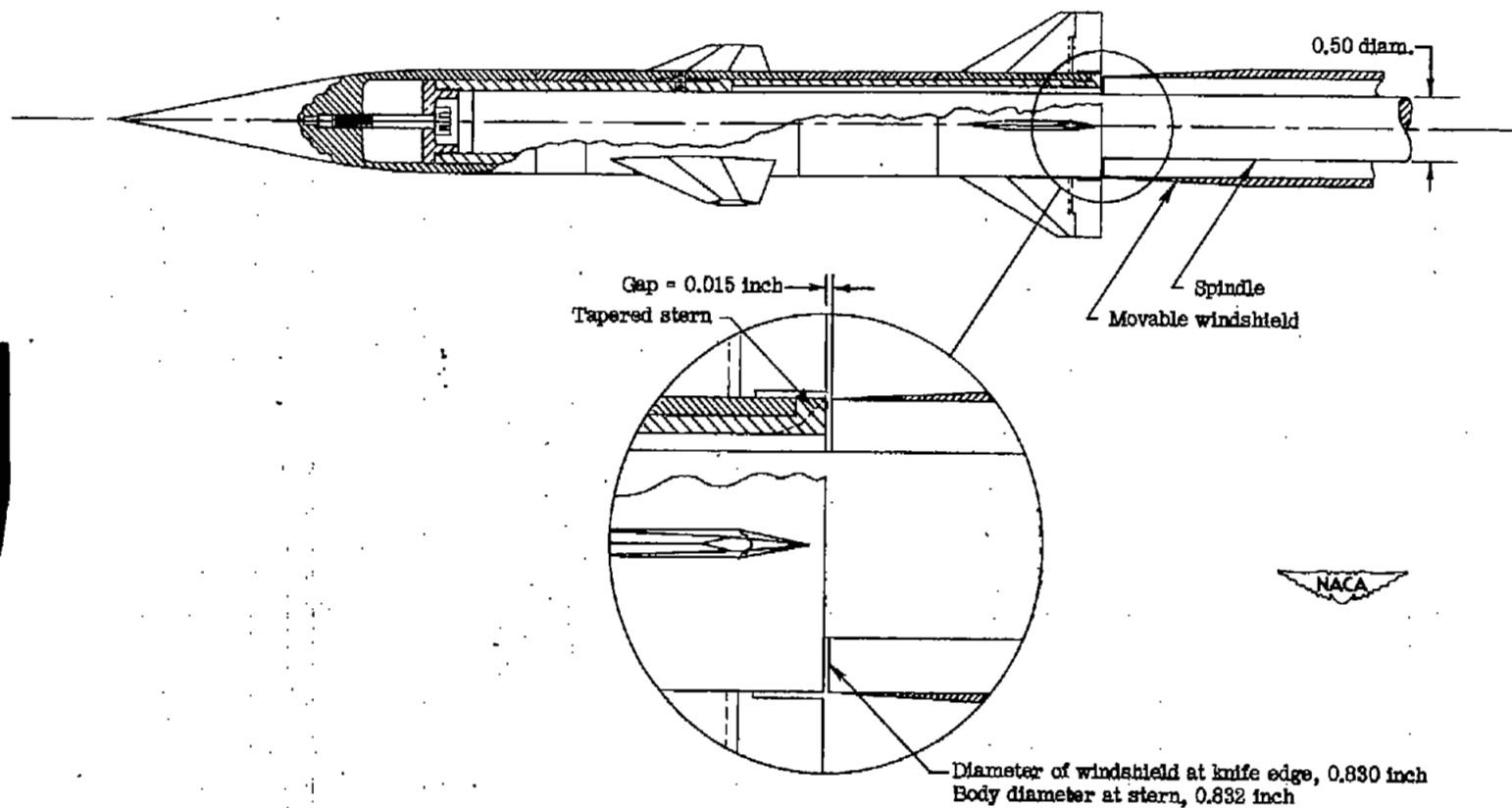


Figure 2.- Cross section of model body and stern detail.

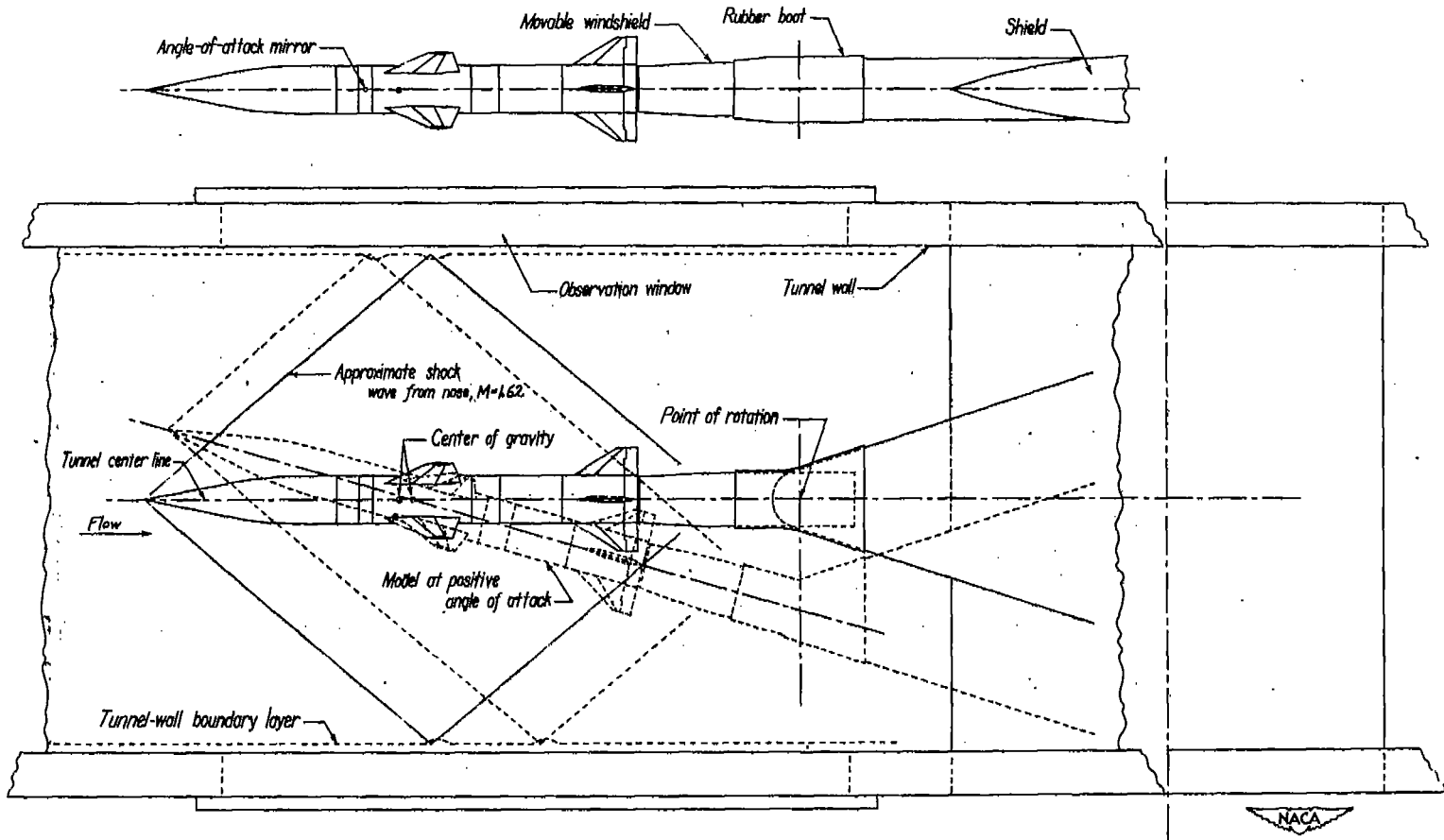


Figure 3.- Model installation in tunnel showing approximate disturbance limits.

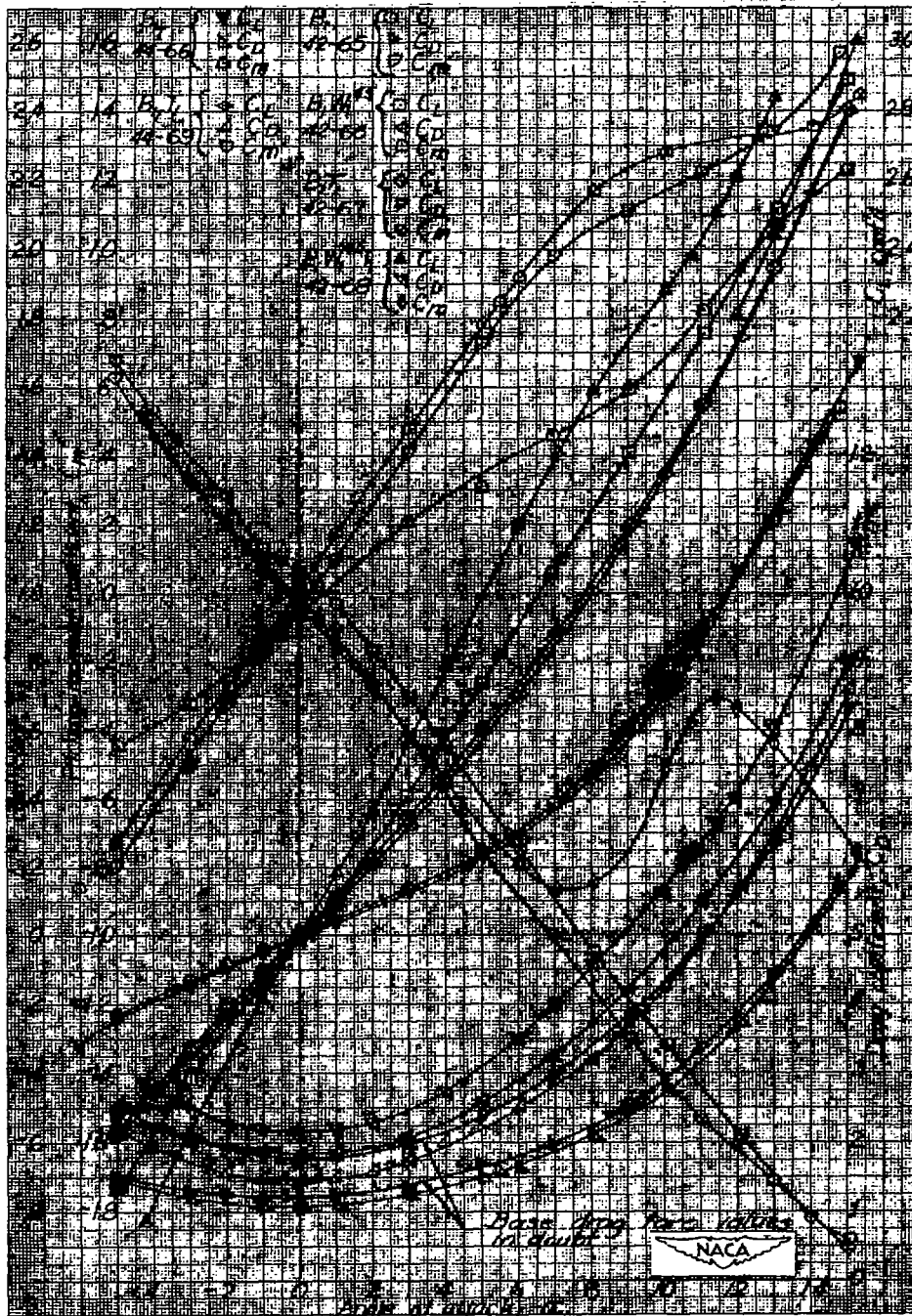


Figure 4.- $M = 1.93$: W_1^{45} and T_1 increments on B_1 , effect of tapered stern on B_1 and $B_1 T_1$, and complete $B_1 W_1^{45} T_1$.

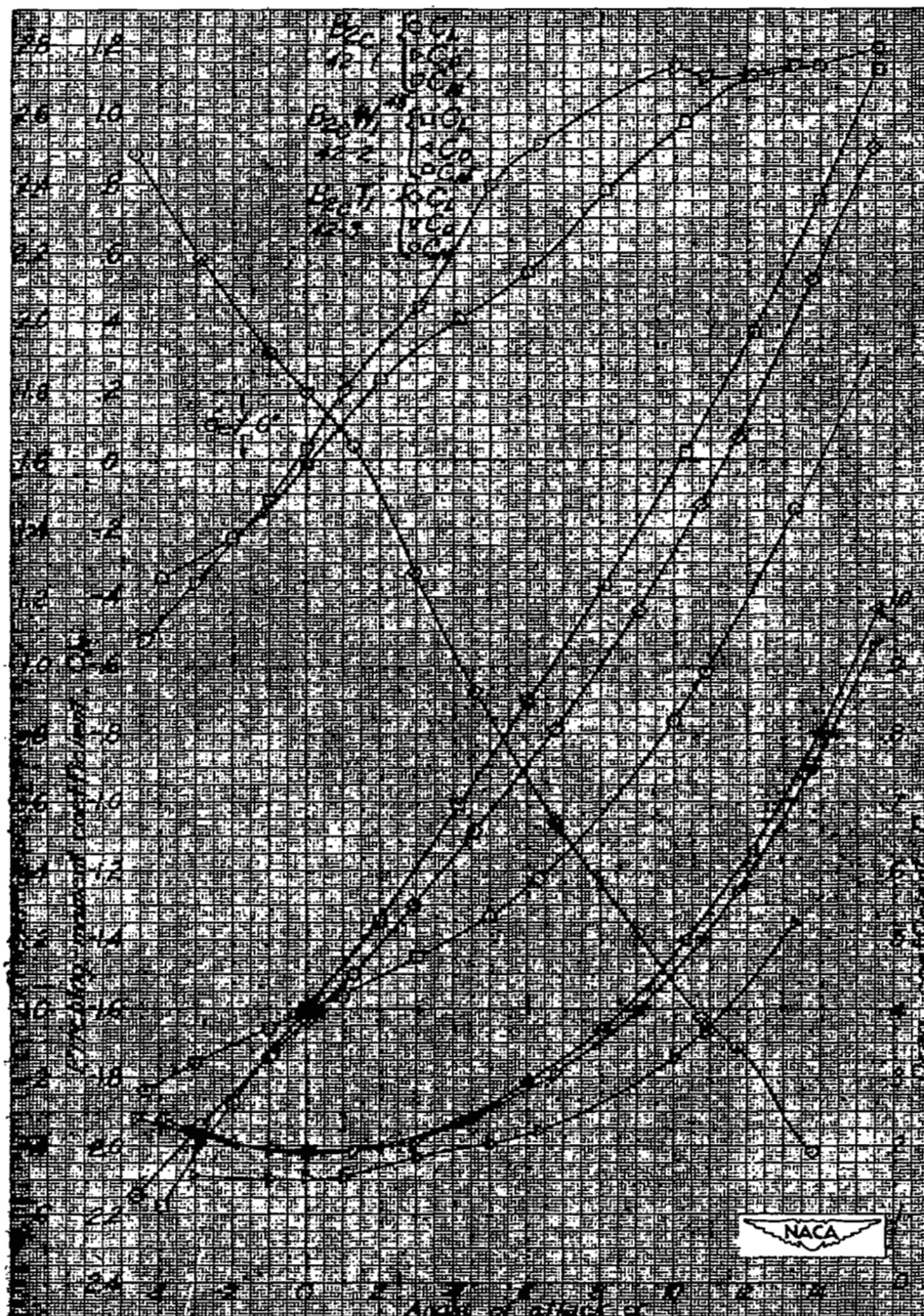


Figure 5.- $M = 1.93$: W_1^{45} and T_1 increments on B_{2c} .

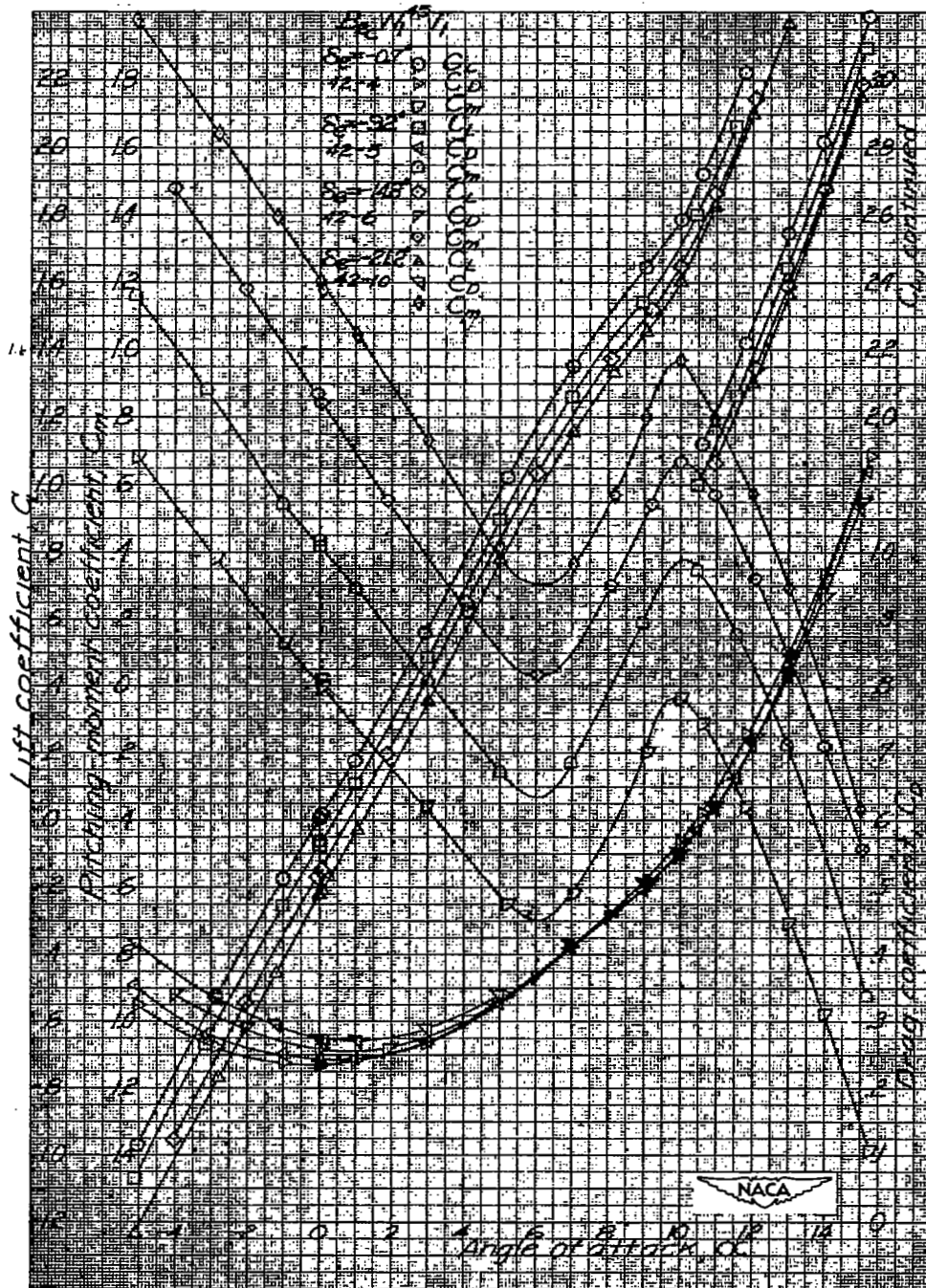


Figure 7.- $M = 1.93$: Effect of elevator deflection on $B_2C W_1^{45} T_1$.

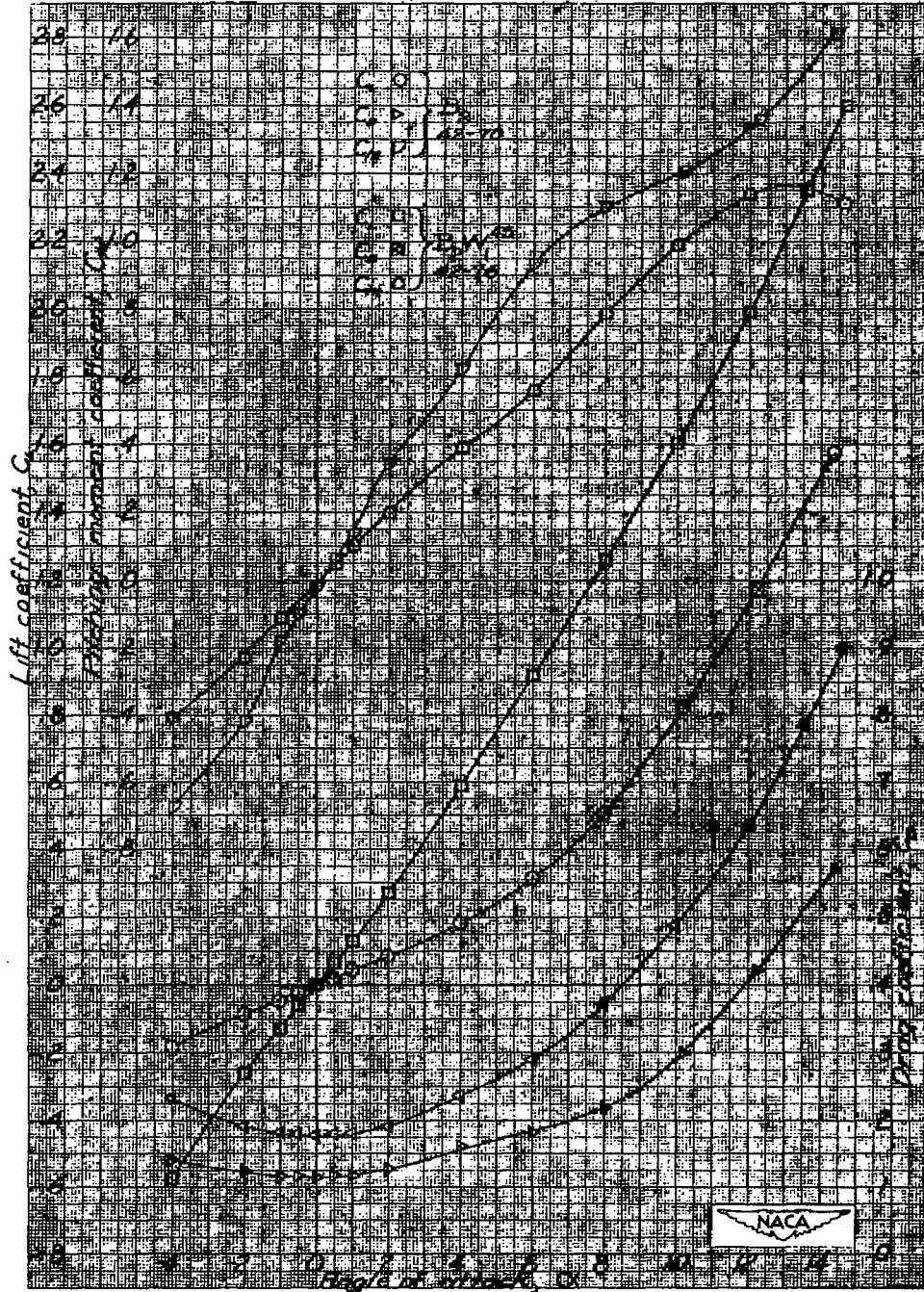


Figure 8.- $M = 1.93$: Basic B_2 characteristics and W_1^{45} increments on B_2 .

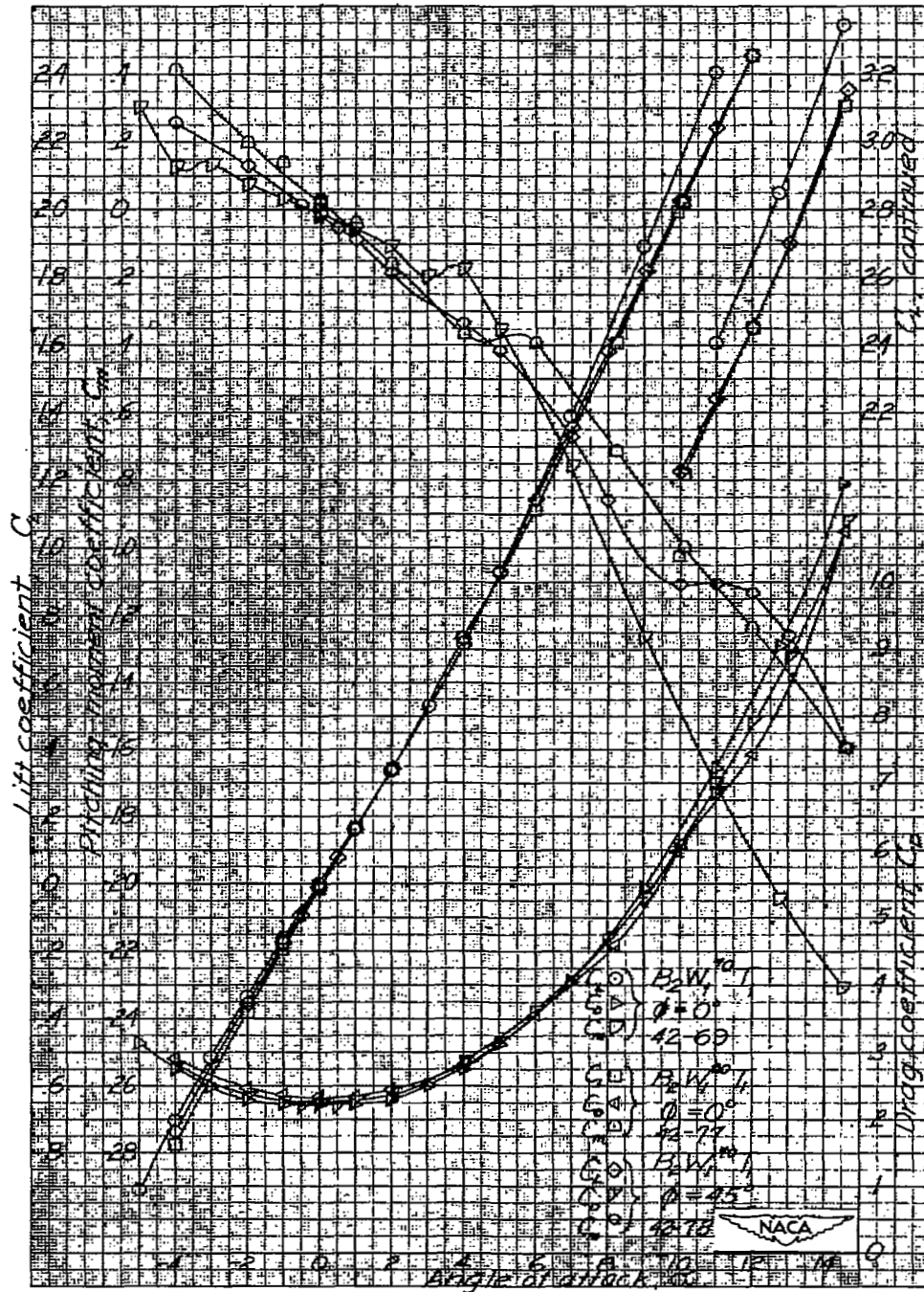


Figure 9.- $M = 1.93$: Effect of varying θ and roll angle on $B_2W_1^{\theta T_1}$.

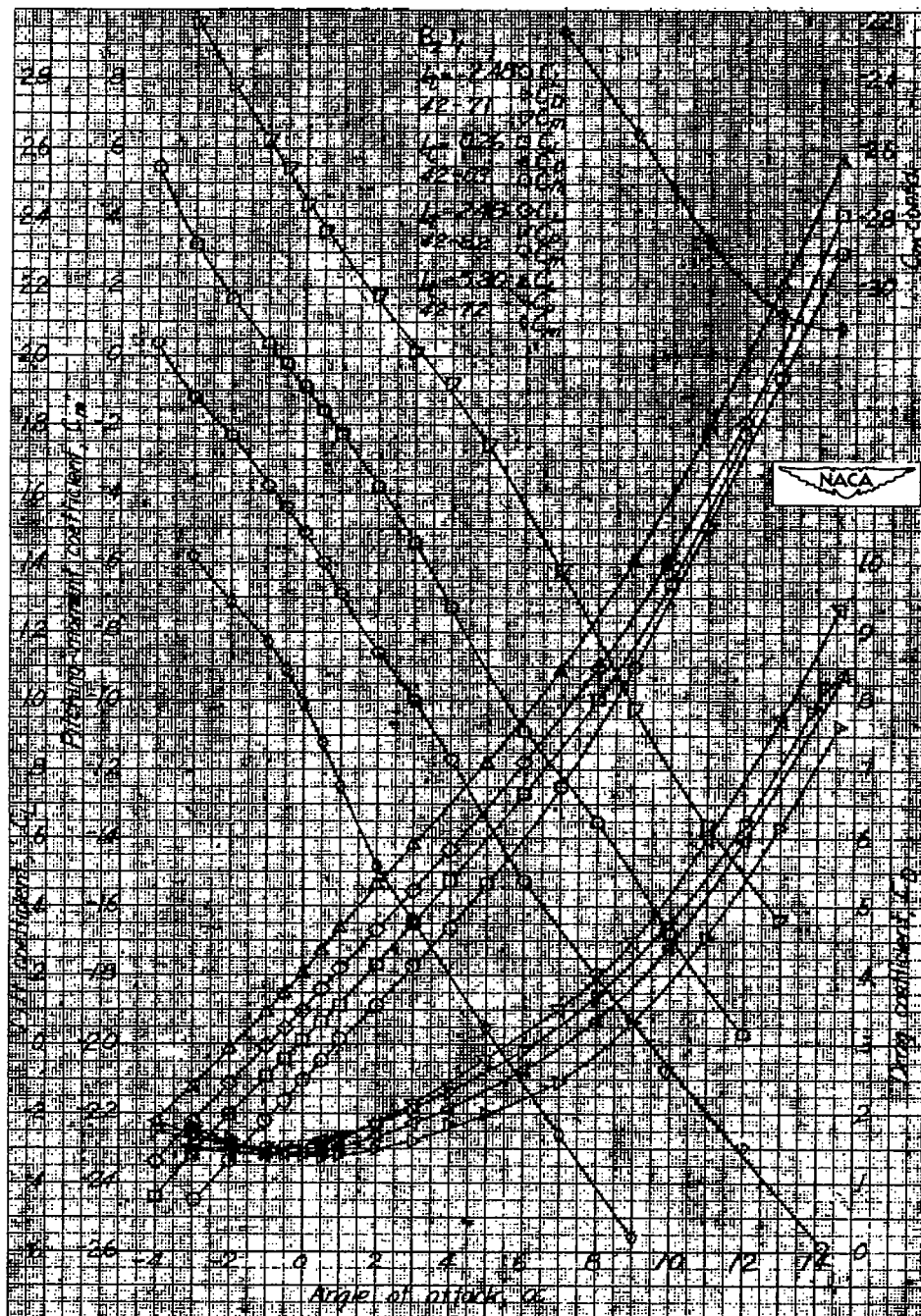


Figure 10.- $M = 1.93$: Effect of varying tail incidence angle in presence of B_2 (to obtain integrated downwash at tail).

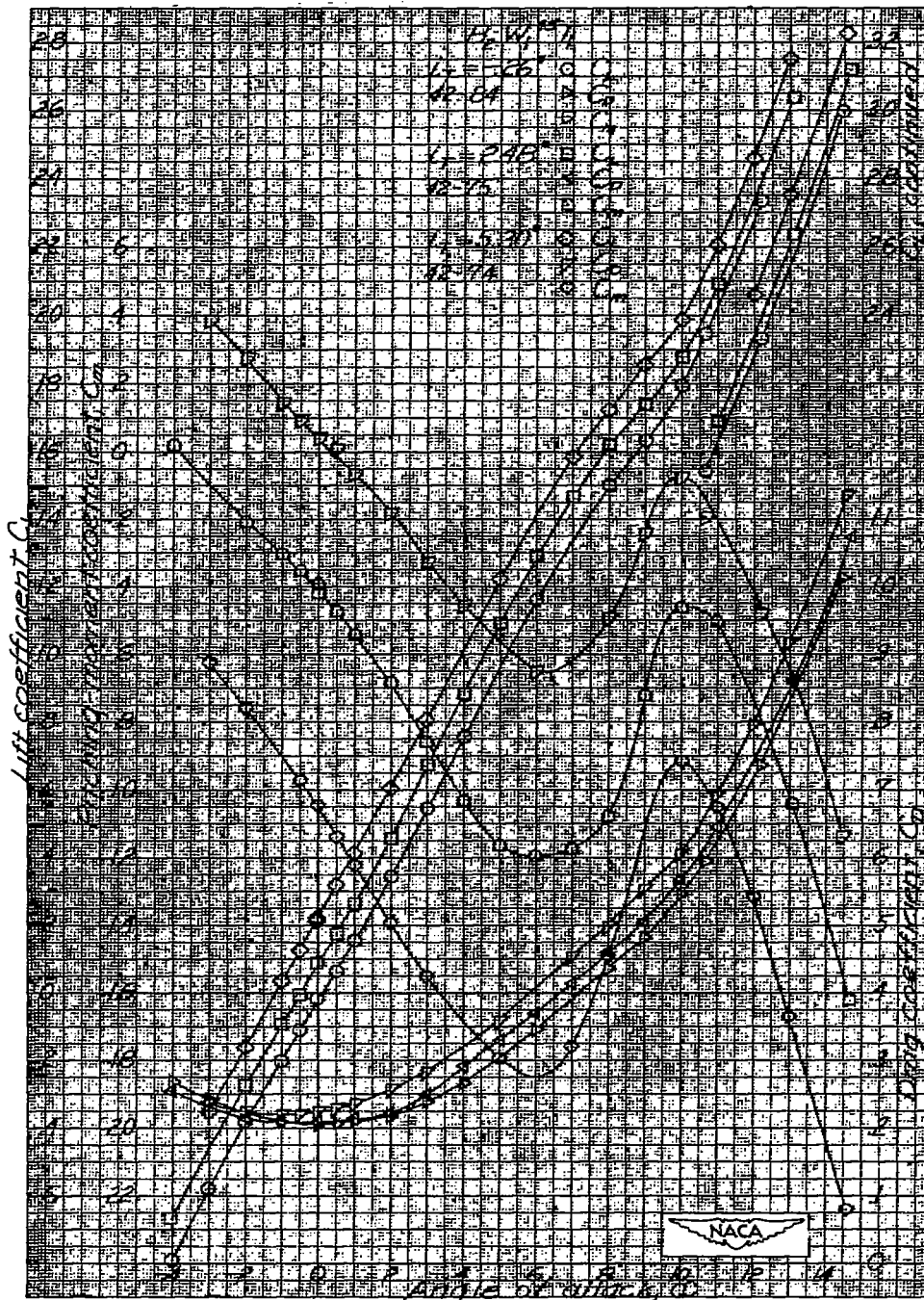


Figure 11.- $M = 1.93$: Effect of varying tail incidence angle in presence of $B_2W_1^{45}$ (to obtain integrated downwash at tail).

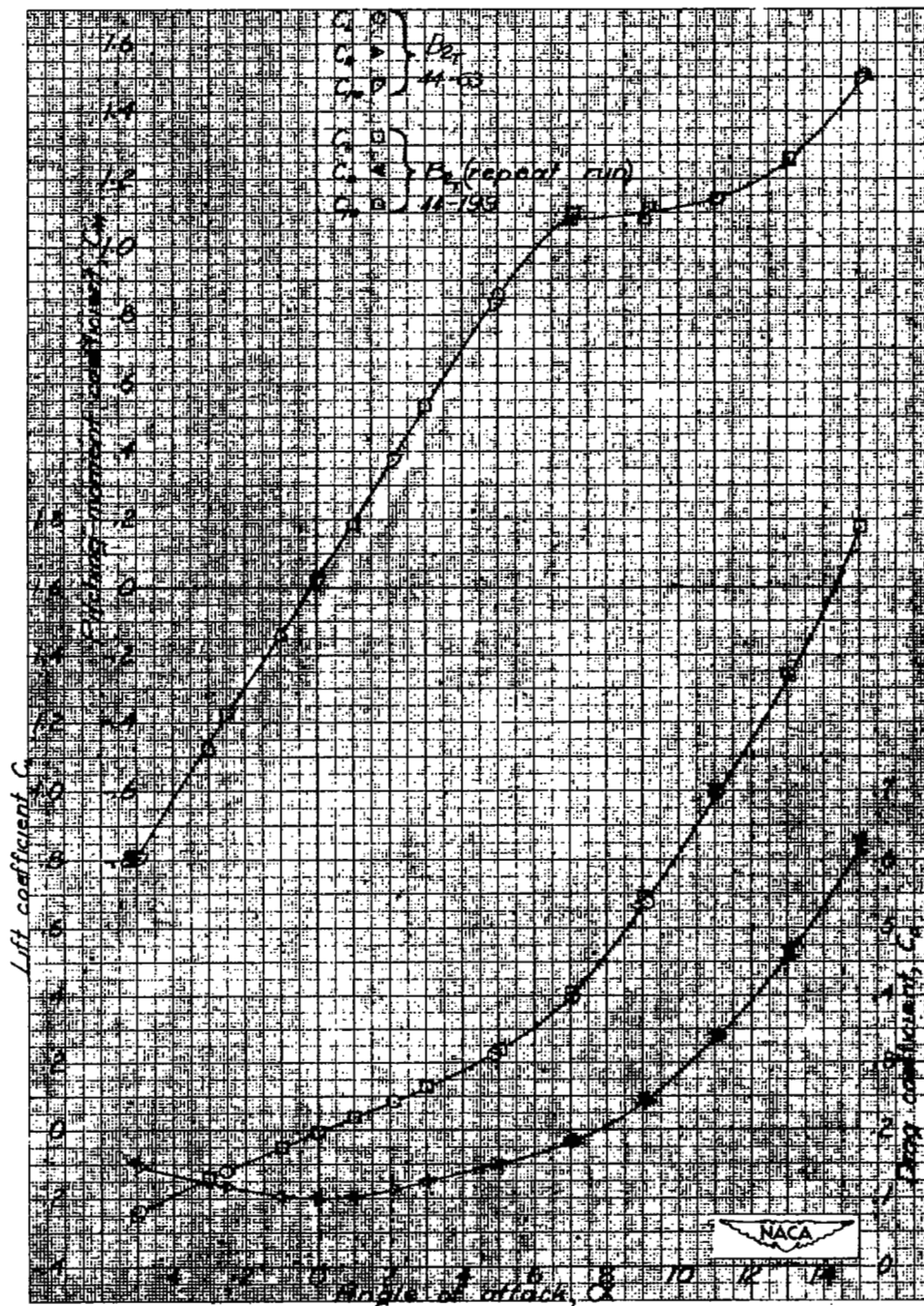


Figure 12.- $M = 1.93$: Basic body characteristics with tapered stern B_{2T} .

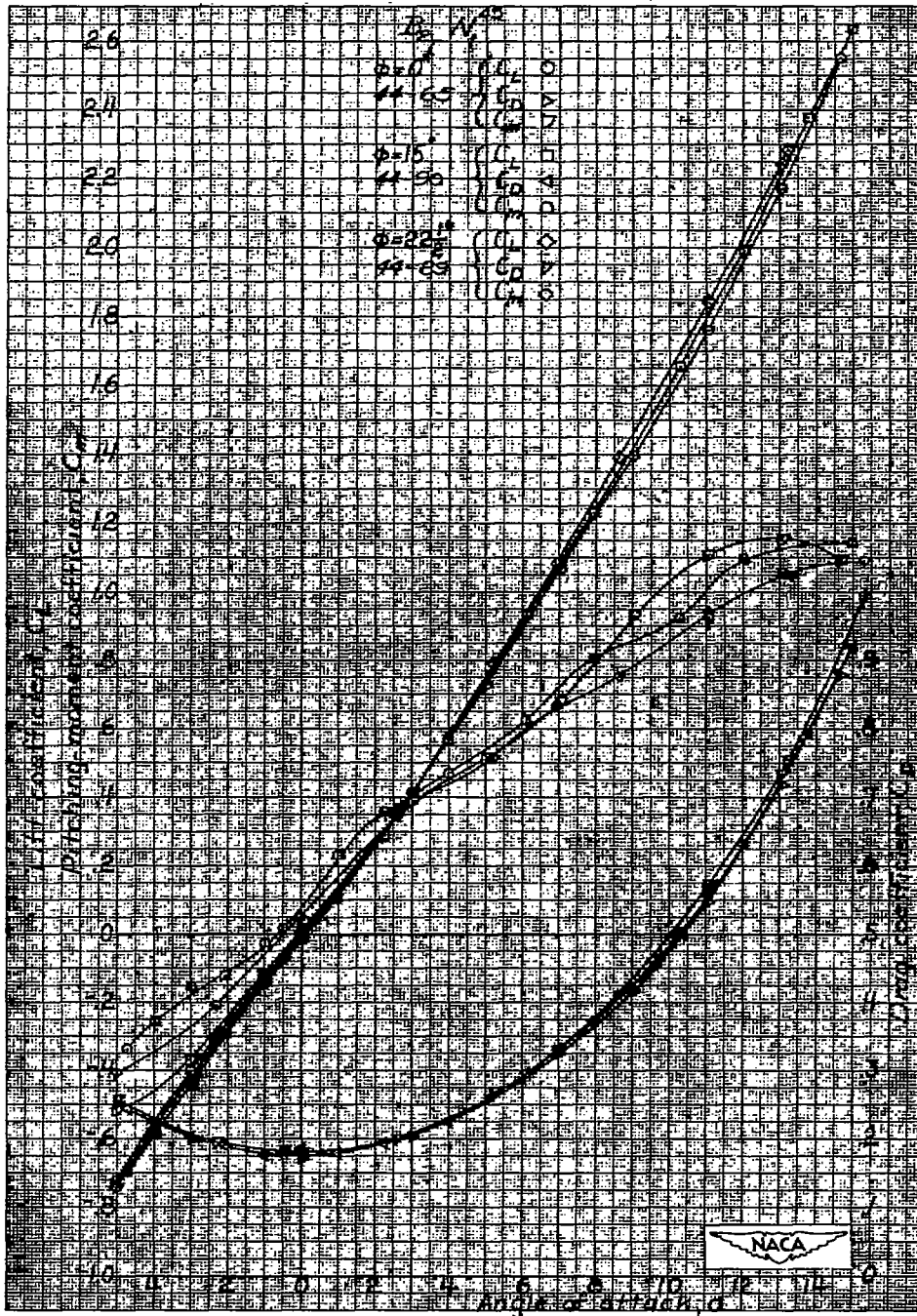


Figure 13.- $M = 1.93$: W_1^{45} increments on B_{2T} at $\phi = 0^\circ, 15^\circ,$ and $22\frac{1}{2}^\circ$.

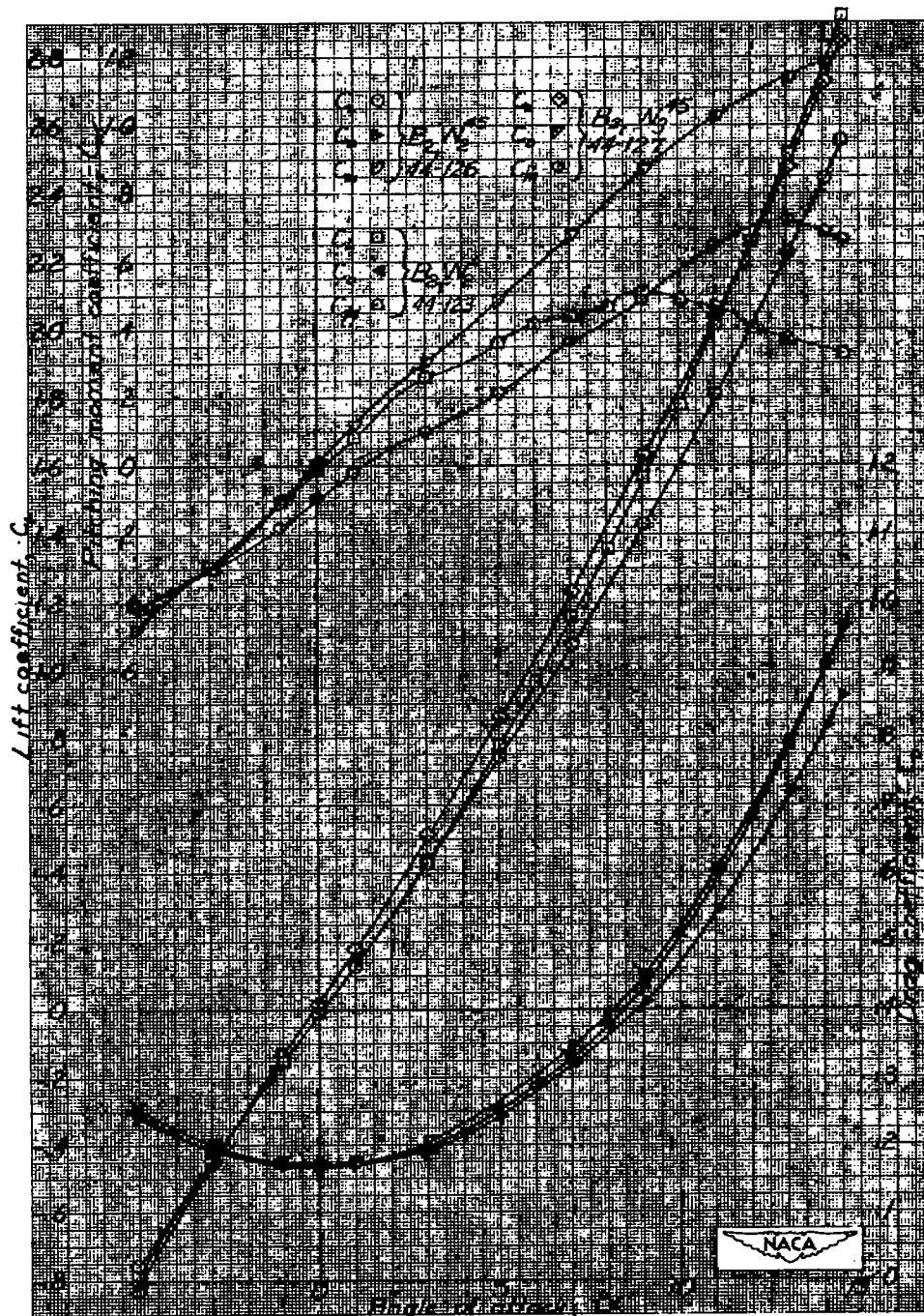


Figure 14.- $M = 1.93$: W_2^{45} , W_2^0 , and W_3^{45} increments on B_{2T}
at $\phi = 0^\circ$.

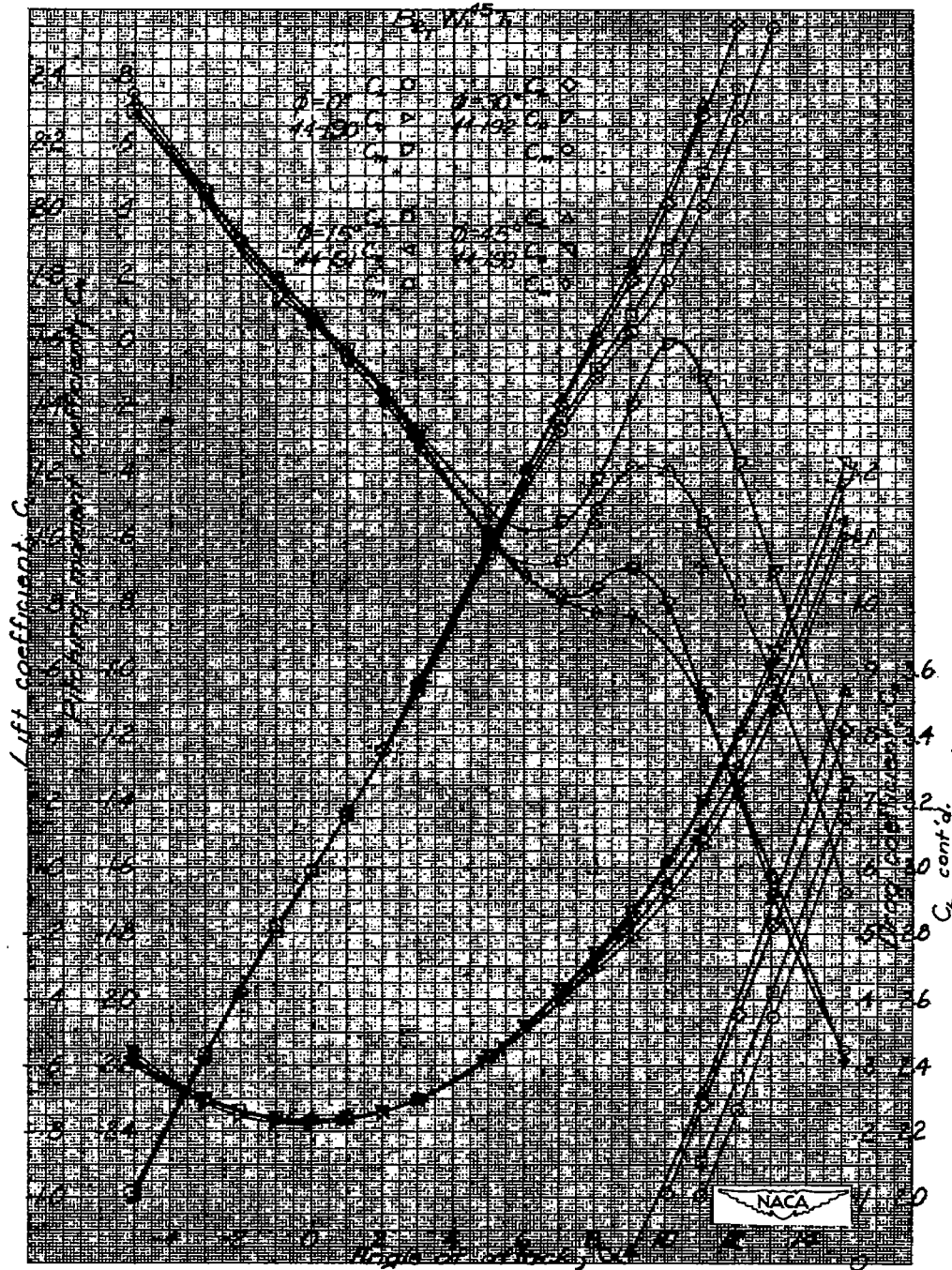


Figure 15.- $M = 1.93$: Effects of roll position on $B_2W_1^{45}T_1$;
 $\phi = 0^\circ, 15^\circ, 30^\circ, \text{ and } 45^\circ$.

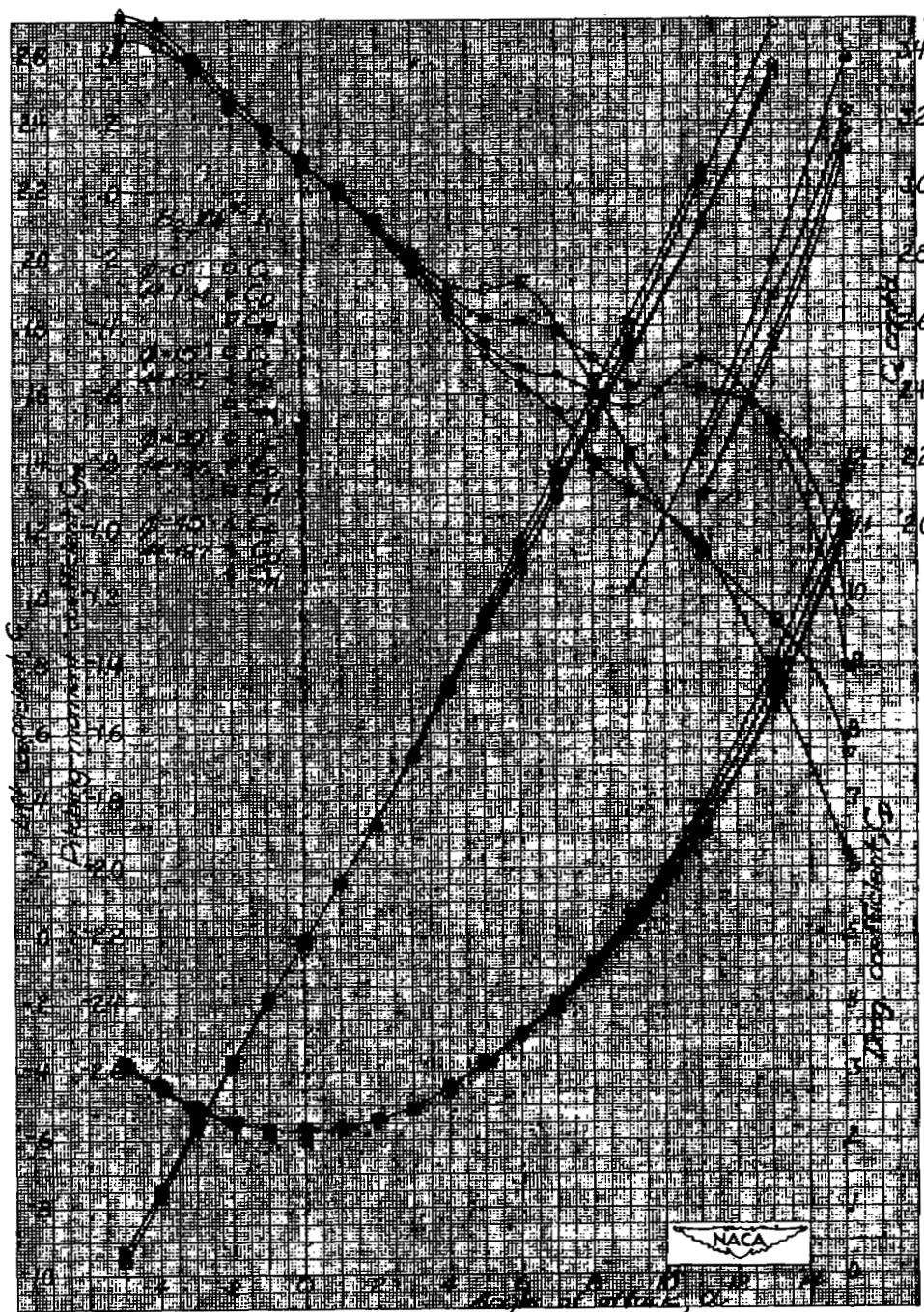


Figure 16.- $M = 1.93$: Effects of roll position on $B_{2T}W_1^{30T_1}$;
 $\phi = 0^\circ, 15^\circ, 30^\circ, \text{ and } 45^\circ$.

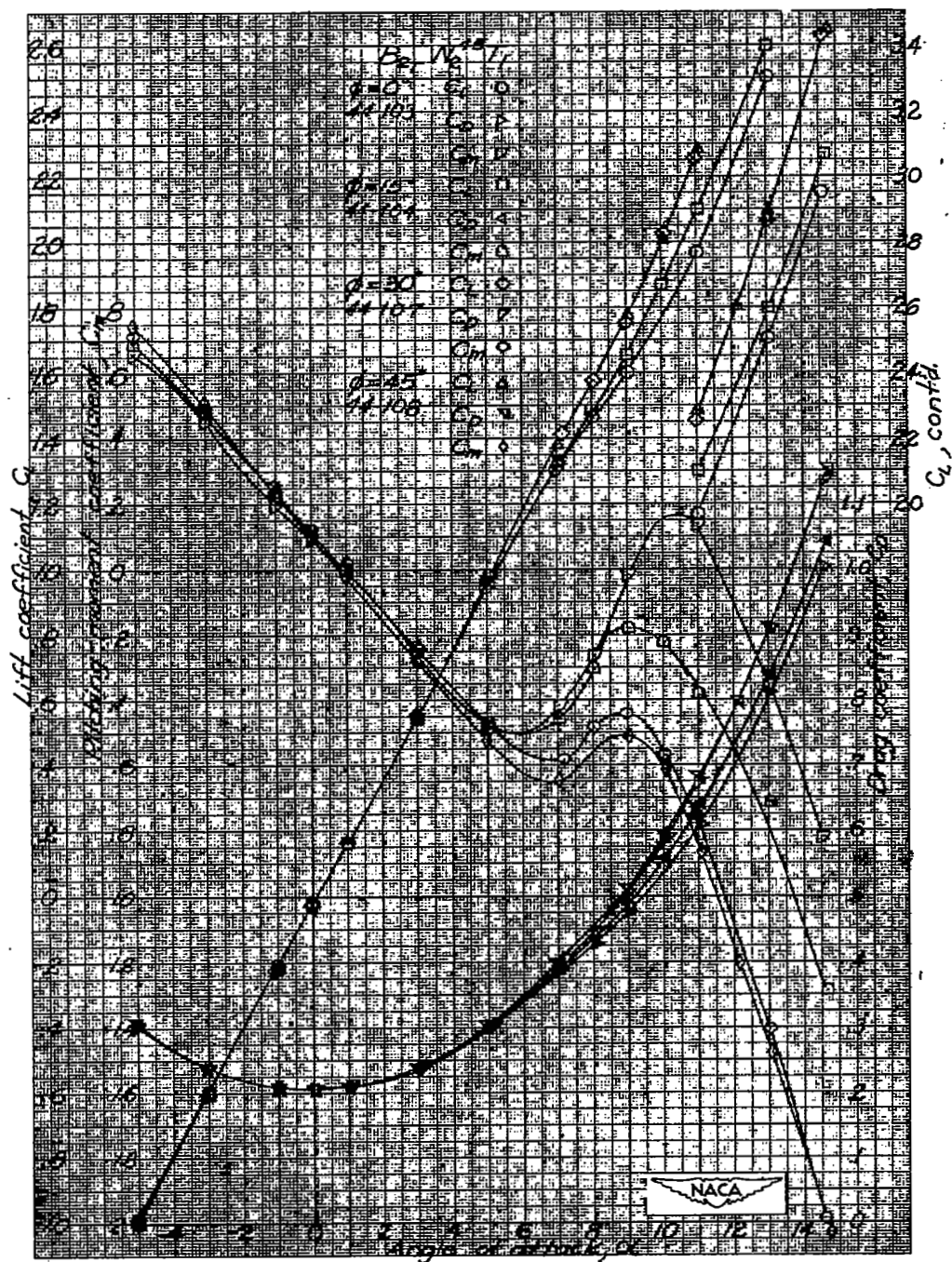


Figure 17.- $M = 1.93$: Effects of roll position on $B_{2T}W_{2}^{45T}T_1$; $\phi = 0^\circ, 15^\circ, 30^\circ, \text{ and } 45^\circ$.

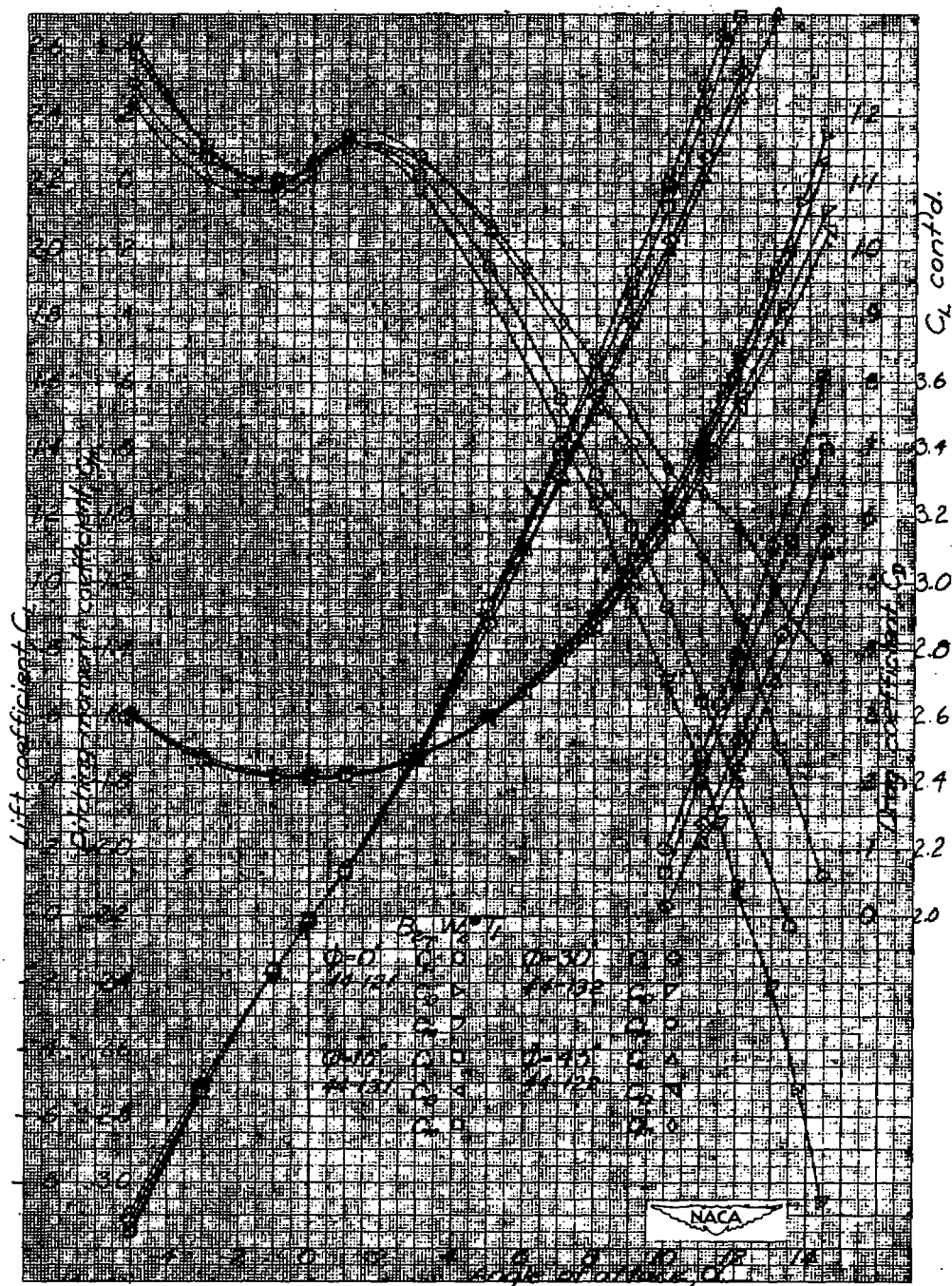


Figure 18.- $M = 1.93$: Effects of roll position on $B_{2T}W_2^0T_{11}$;
 $\phi = 0^\circ, 15^\circ, 30^\circ, \text{ and } 45^\circ$.

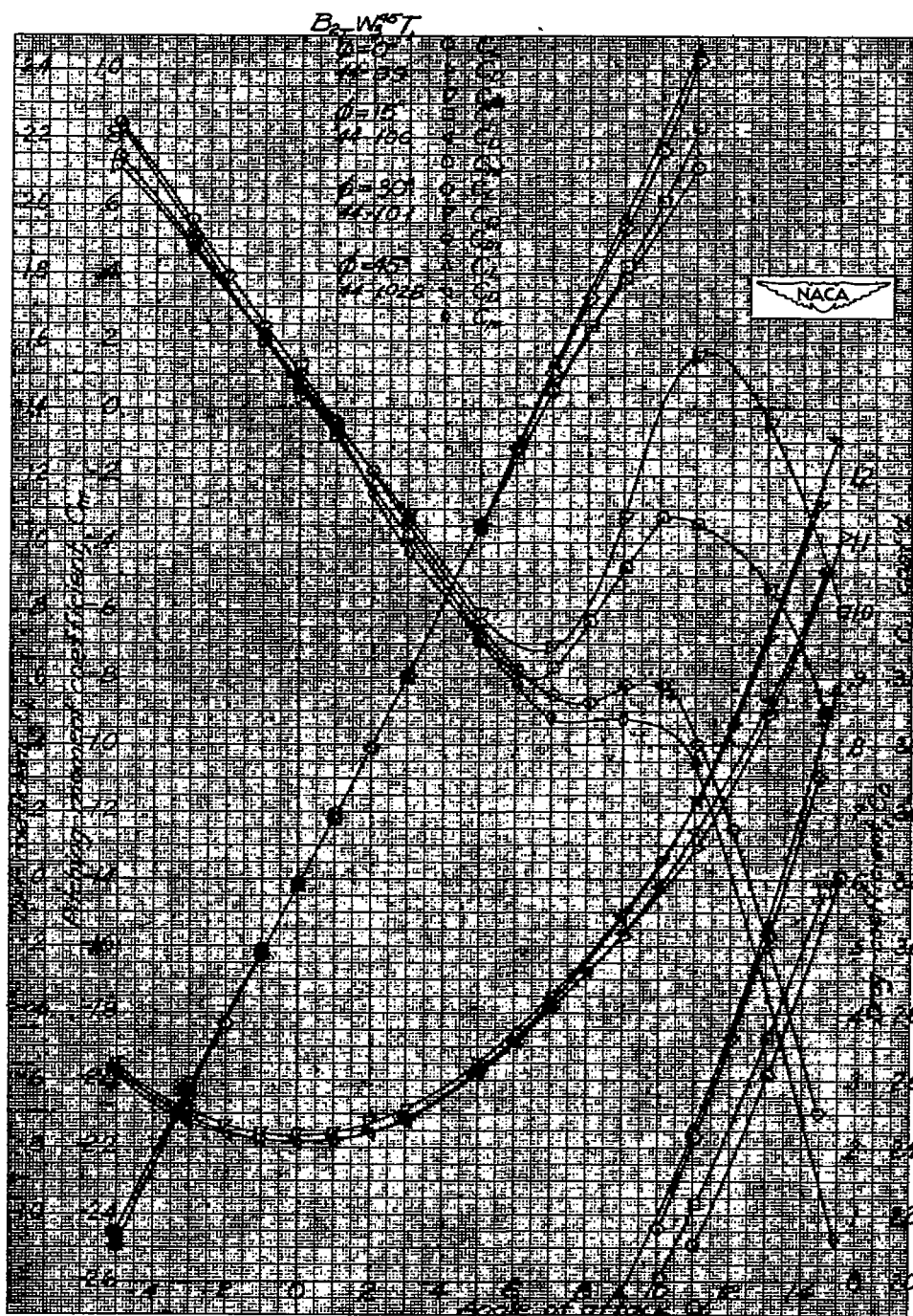


Figure 19.- $M = 1.93$: Effects of roll position on $B_{2T}W_3^{45}T_1$; $\phi = 0^\circ, 15^\circ, 30^\circ, \text{ and } 45^\circ$.

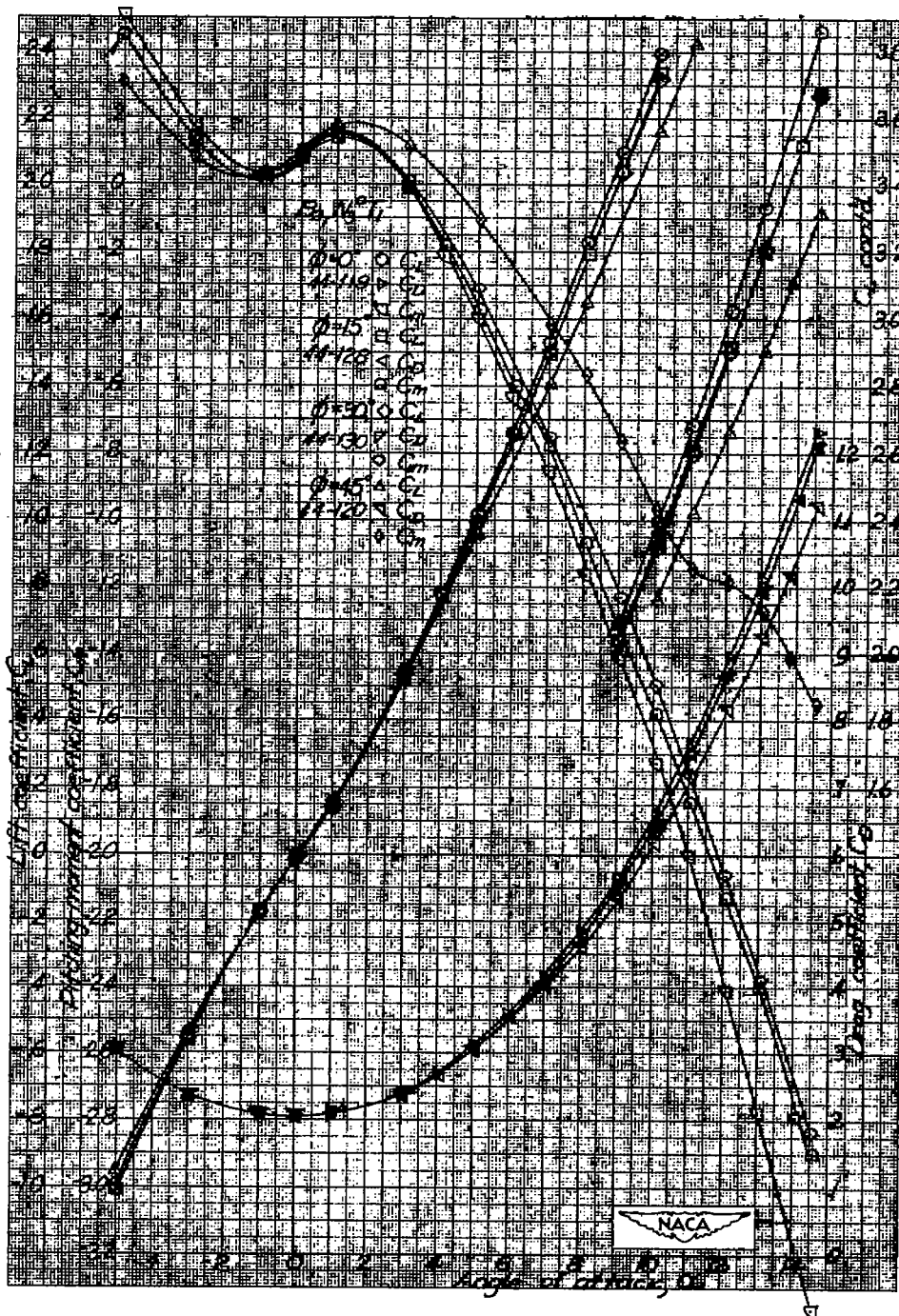


Figure 20.- $M = 1.93$: Effects of roll position on $B_{2T}W_3T_1$;
 $\phi = 0^\circ, 15^\circ, 30^\circ, \text{ and } 45^\circ$.

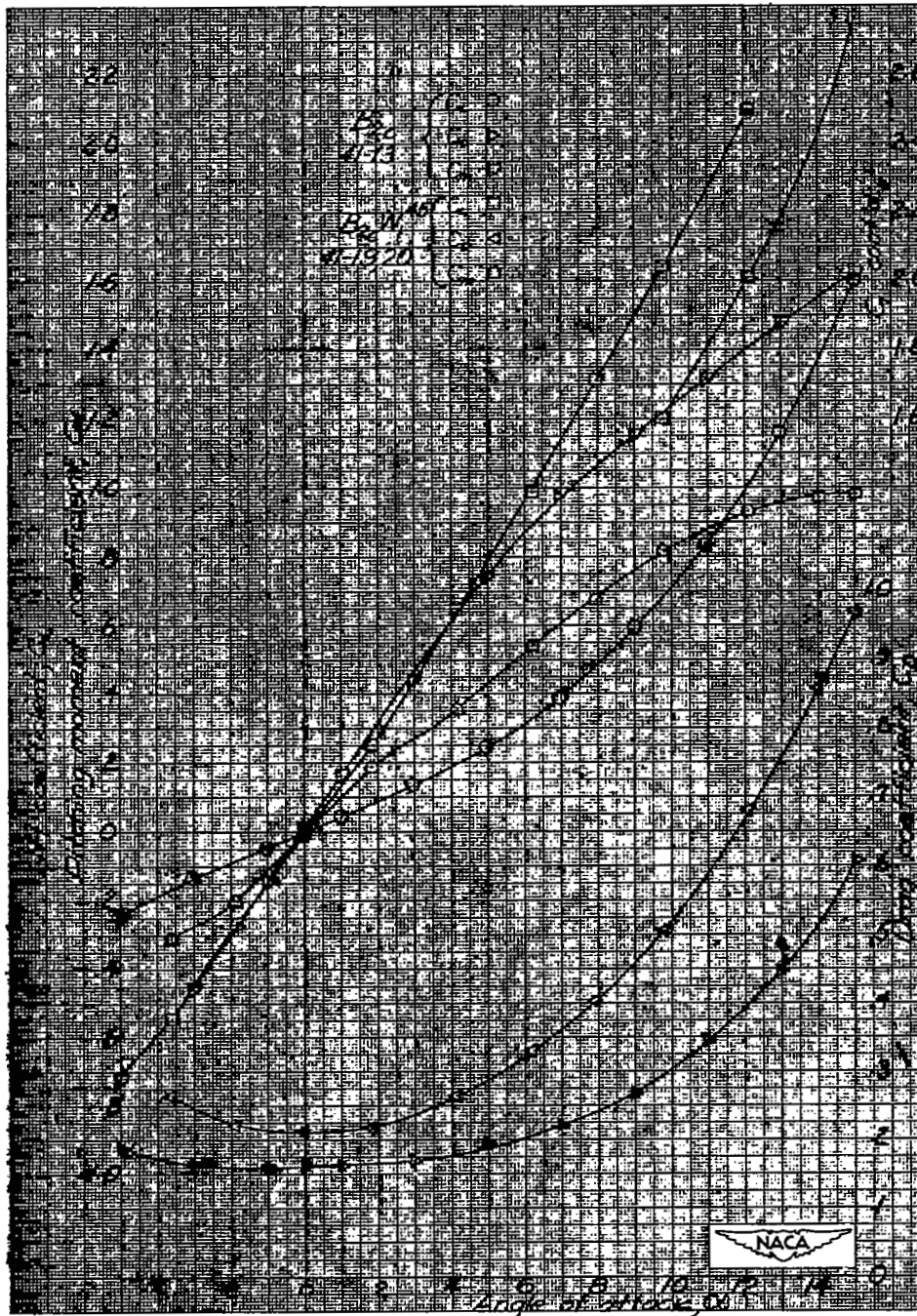


Figure 21.- $M = 1.62$: Basic body characteristics with conduit covers B_{2c} and W_1^{45} increments in presence of B_{2c} .

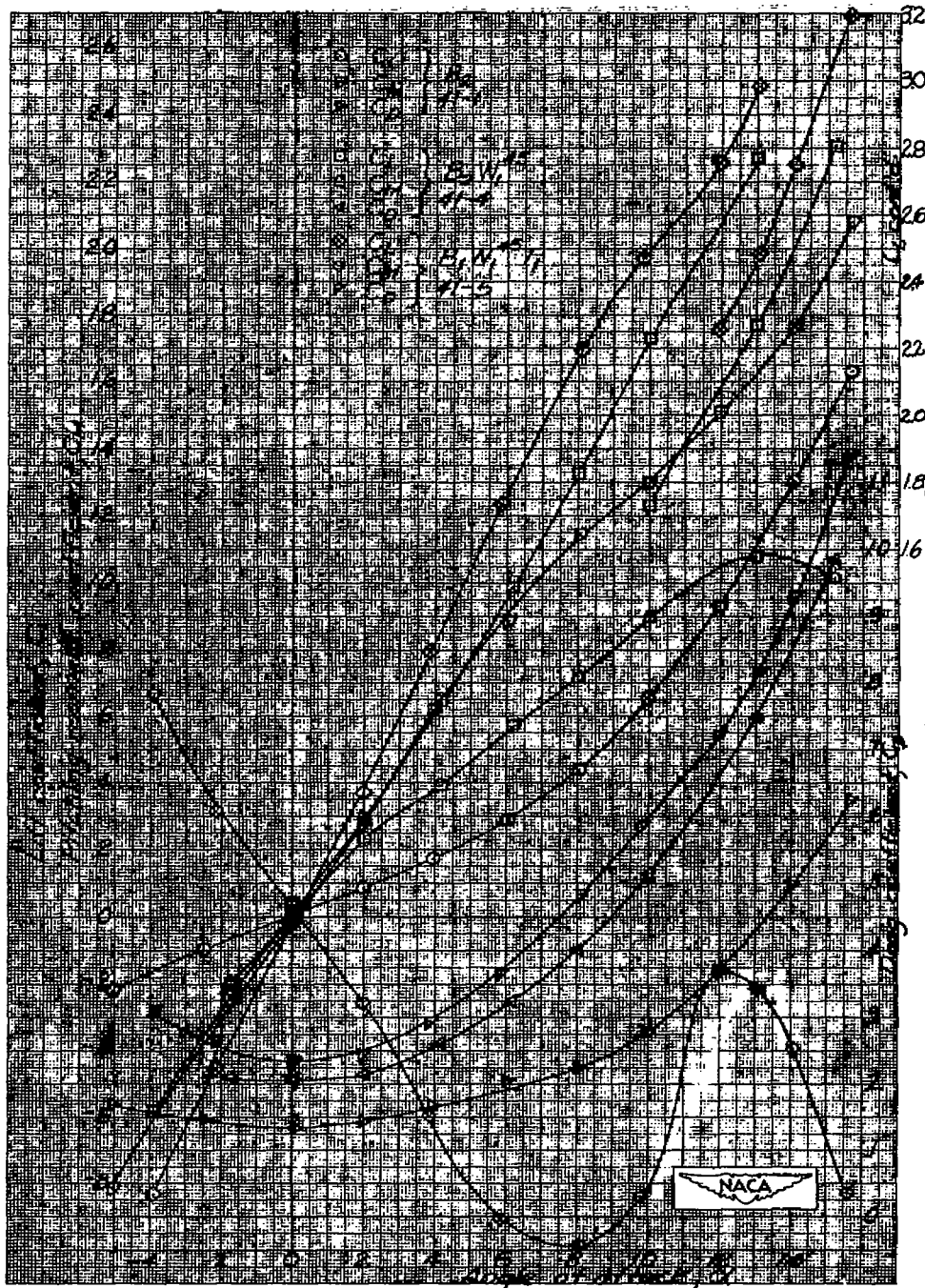


Figure 22.- $M = 1.62$: Basic B_2 characteristics, W_1^{45} increment, and complete $B_1W_1^{45}T_1$.

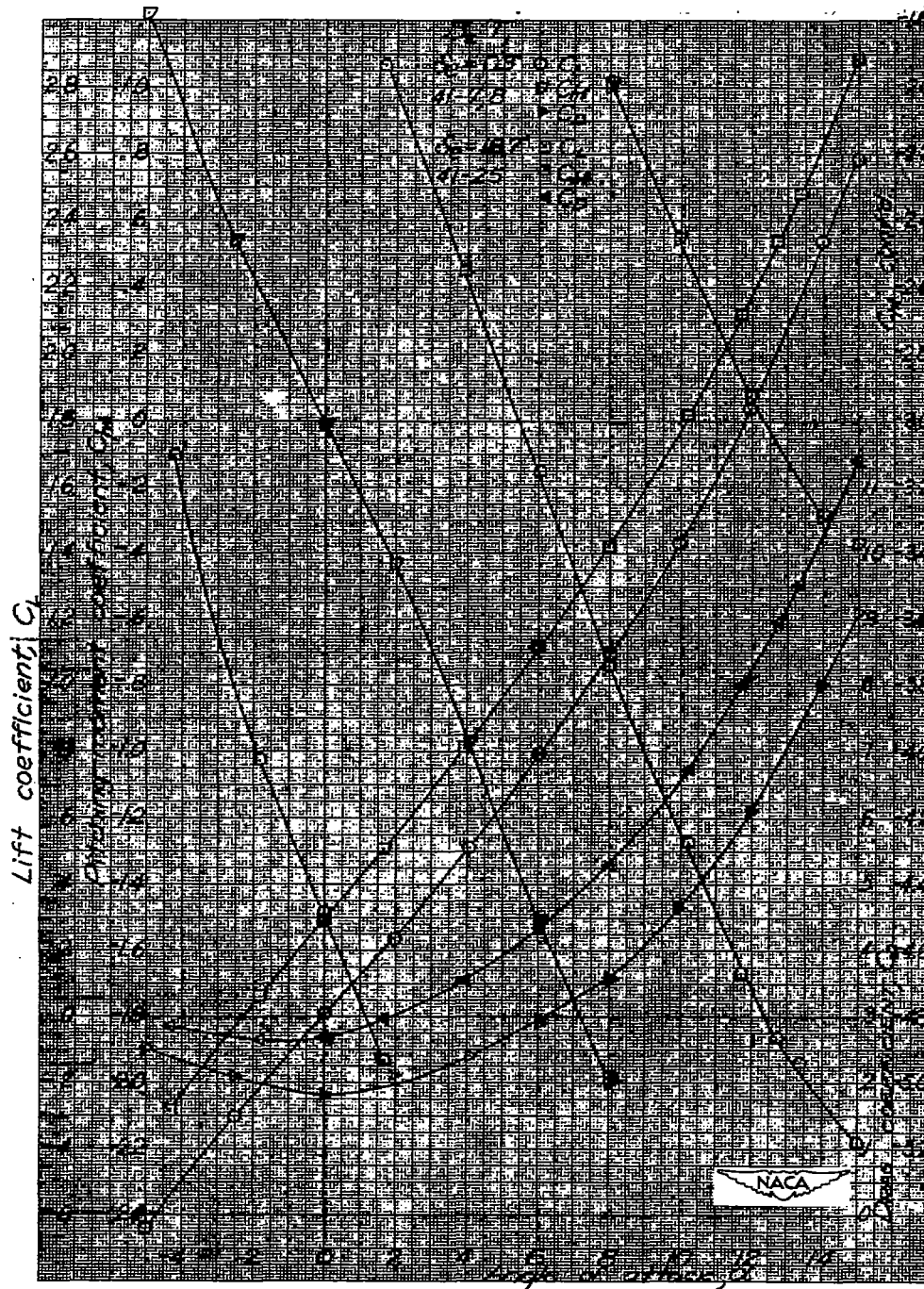


Figure 23.- $M = 1.62$: Effects of elevator deflections of T_1 in presence of B_2 .

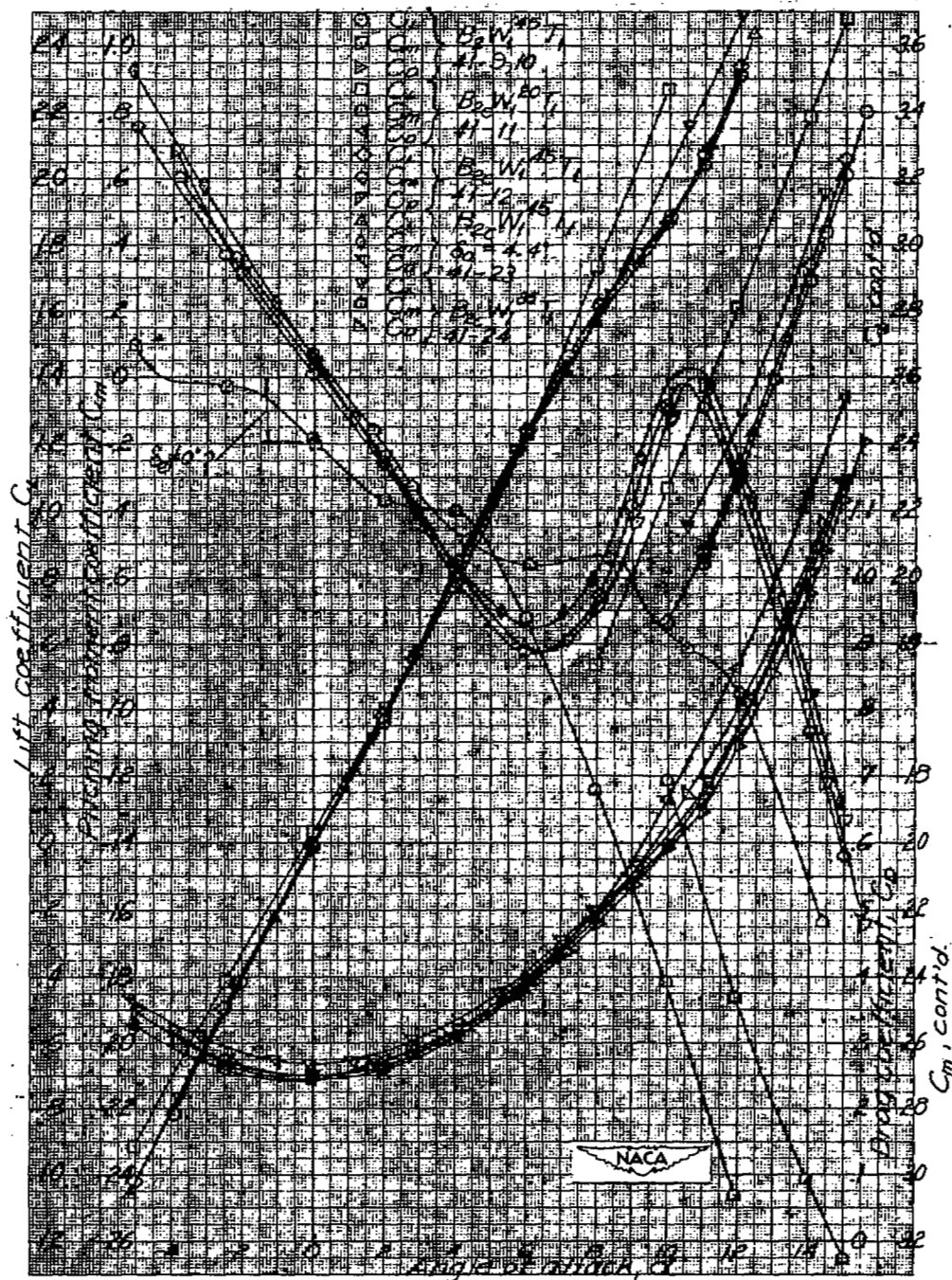


Figure 24.- $M = 1.62$: Effect of adding conduit covers, varying θ , and introducing a static rolling moment on $B_2W_1^{45}T_1$.

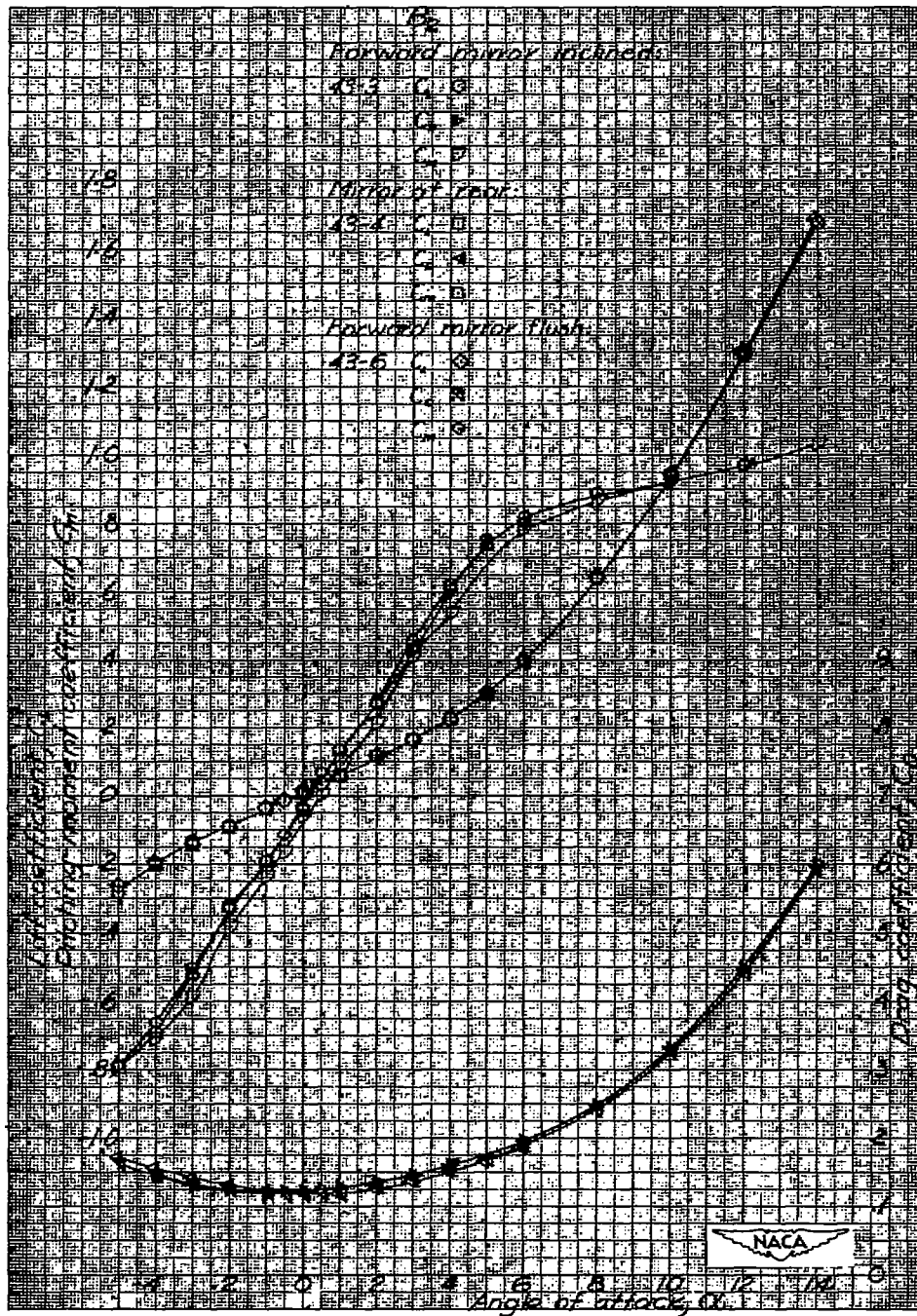


Figure 25.- $M = 2.40$: Effects of angle-of-attack mirror location on basic B_2 characteristics.

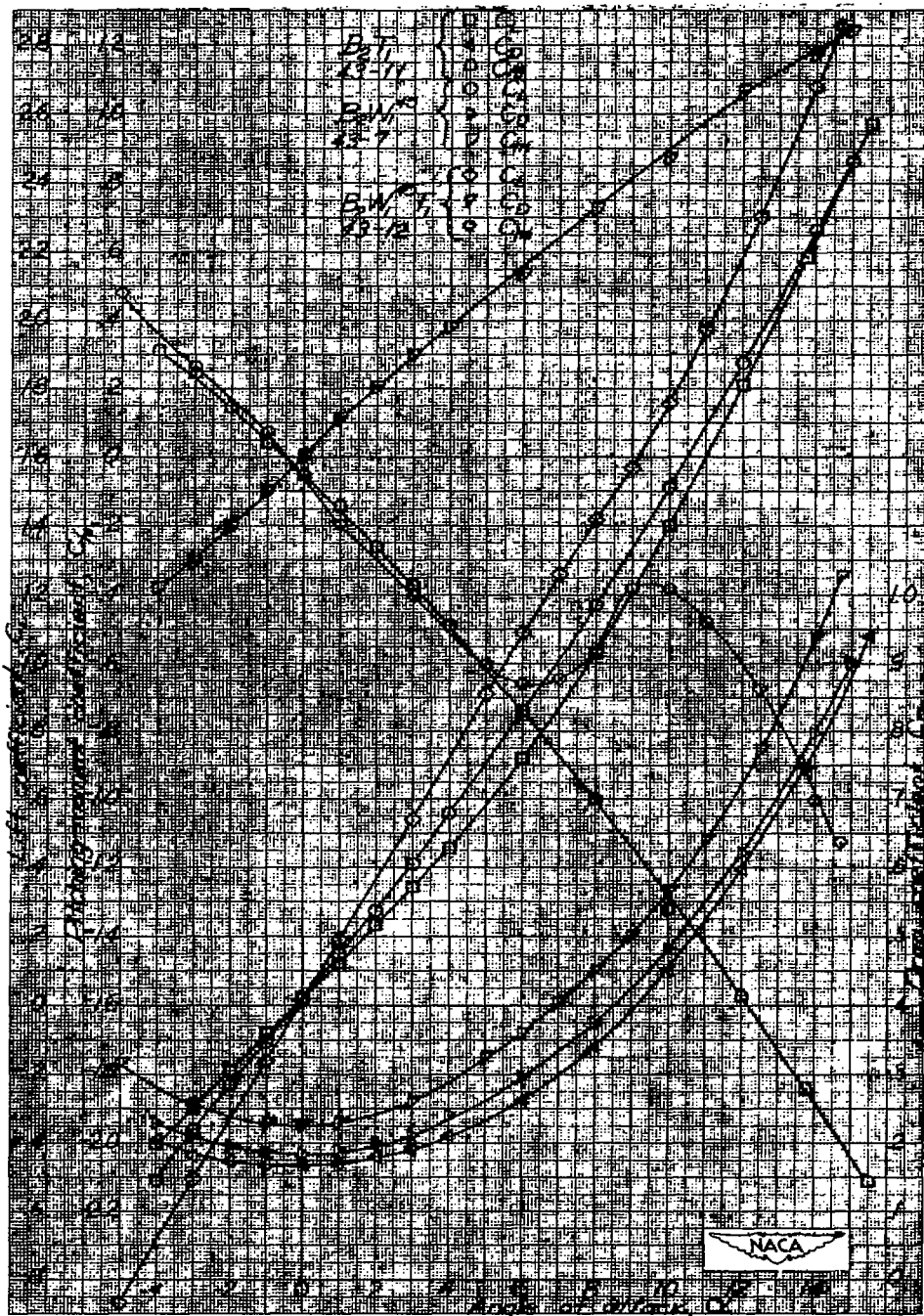


Figure 26.- $M = 2.40$: W_1^{45} and T_1 increments on B_2 and complete $B_2W_1^{45}T_1$.

NASA Technical Library



3 1176 01436 3007

